Supersonic Vehicle Configuration Transitions To Enable SRP During Mars EDL

David J. Blette and Robert D. Braun
Georgia Institute of Technology, Atlanta, Georgia 30332

Background and Motivation

Supersonic retropropulsion (SRP) is an enabling technology for landing high mass payloads on Mars. Recent efforts to develop the state of the art of SRP have primarily focused on SRP system performance during EDL, propulsive-aerodynamic interaction characterization, and CFD modeling capability development.

The vast majority of SRP analyses ignore the challenges and impacts of supersonically transitioning a hypersonic entry vehicle configuration into a vehicle configuration that allows for SRP steady-state operation.

- Configuration transitions impact EDL timeline events and landed mass capabilities.
- Recent analyses have assumed free-fall time penalties before SRP initiation to conservatively account for transition impacts on the EDL timeline.

Challenges

All Mars atmospheric vehicle transitions to-date have occurred subsonic and relied on subsonic free-fall assumptions to mitigate debris recontact risks during solid mass ejections.

- Due to fundamental differences between supersonic and subsonic fluid flows, separation complexity and risk are increased during supersonic transitions.
- Transitions involving mass jettisons pose near-field and far-field recontact risks to the descent vehicle.
- To advance SRP to a flight-ready status, analysis is required to characterize the unique challenges of supersonic transitions.

Baseline Mission and Analysis

The entry vehicle design considered in this study closely resembles that of the EDL-Systems Analysis Architecture 1 [Dwyer]:

- 10x30m rigid mid-L/D hypersonic aeroshell
- 110 mT entry mass
- L/D~0.6 at 35º AOA
- Supersonic and subsonic propulsive deceleration

Reference Transition Architectures

Proposed vehicle configuration transitions aim to minimize overall complexity, risk, and required propellant mass during SRP

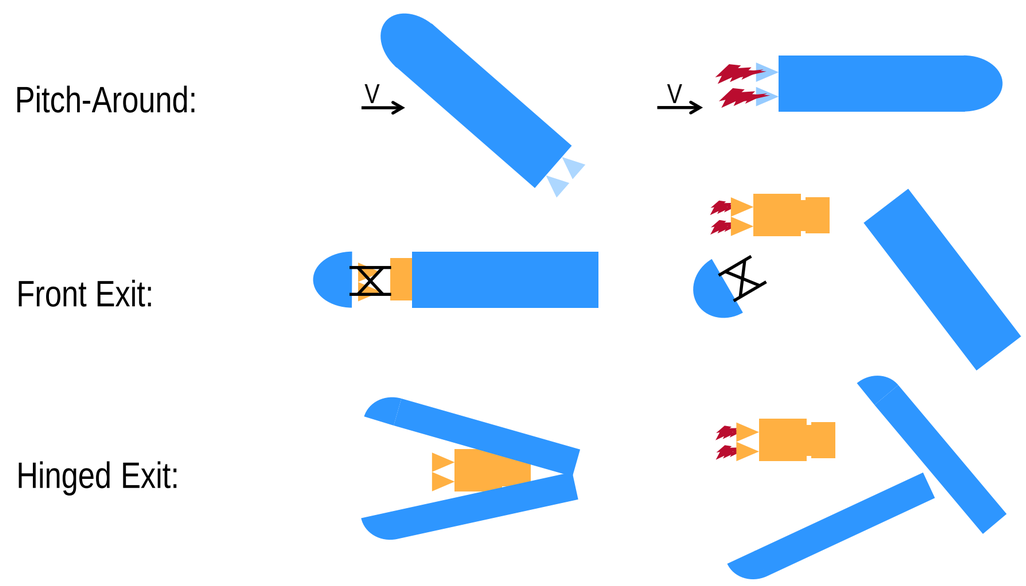

Proposed Analysis and Expected Outcomes

The 3 transition architectures will be compared according to:

- Time to complete transition
- Required subsystem performance
  - RCS and ejection system thrust capability
  - Mass (mechanical and propulsive)
- Altitude-velocity performance

Expected outcomes:

- Provide recommendation for transition architecture
- Bound transition times
- Bound required transition subsystem mass and performance

Preliminary Pitch Maneuver Results

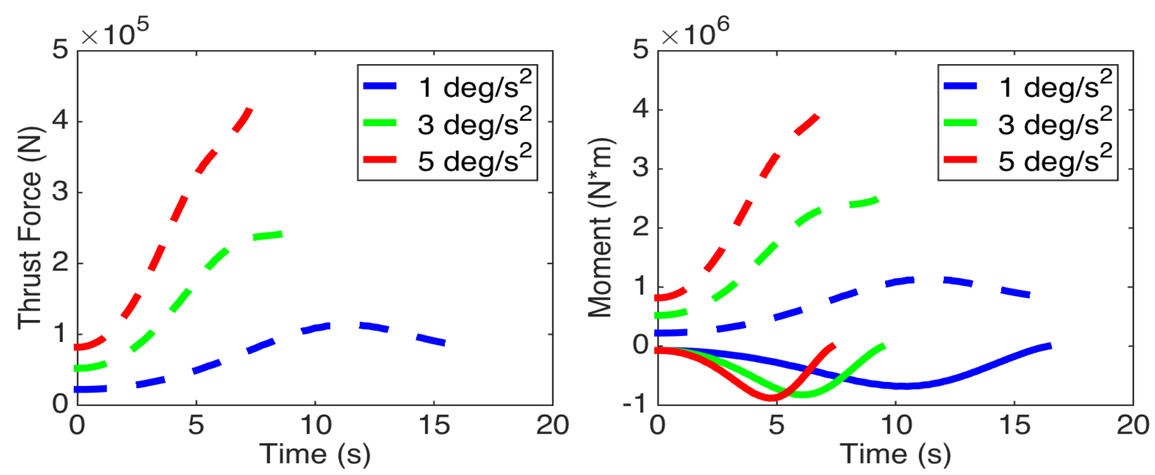

(*Left*) – RCS thrust force required to perform a pitch-around maneuver for varying angular accelerations.
(*Right*) – Aerodynamic moments (solid) and required moments due to thrusters (dashed) to perform a pitch-around maneuver for several angular accelerations.
Initiation Conditions: Mach 3.35, 8.7 km altitude

Conclusions:

- Higher angular accelerations result in faster transition times but require more powerful thrusters to perform the maneuver.
- Commanding an angular acceleration of 5 deg/s^2 requires prohibitively large RCS thrusters (~400 kN). Improvements can be made by limiting angular velocity during the maneuver.
- Accelerations on the order of 1 deg/s^2 result in plausible performance requirements on RCS thrusters (~100 kN).
- 20 seconds is a conservative estimate of supersonic vehicle configuration transitions utilizing a pitch-around maneuver.

Acknowledgments and References

Funding for this work is generously provided by a NASA Space Technology Research Fellowship. A special thanks to Dr. Robert Braun and Dr. Chuck Campbell for their guidance and advice. Some images in this presentation are modified from the EDLSA Phase 1 report.

References:

- Dwyer Cianciolo, A.M., et al., (2010) *Entry, Descent and Landing Systems Analysis Study: Phase 1 Report.*

Trajectory Analysis of an Atmospheric Breathing Supersonic Retropropulsion (AB-SRP) Vehicle to Land Heavy Payloads on Mars

Keir Gonyea
Dr. Robert Braun
Georgia Institute of Technology
Dr. Aaron Auslender
NASA Langley Research Center

Space Systems Design Laboratory

Abstract

Design and analysis of an atmospheric breathing supersonic retropropulsion system to land large-scale spacecraft (10+ MT) on Mars was performed. A simulation was developed to simulate the supersonic and subsonic phases of descent following hypersonic entry using a mid-lift-to-drag ratio elliptical sled. The ability of the atmospheric breathing retropropulsion system to land a 40 MT, human-scale payload on Mars was compared to that of a traditional supersonic retropropulsion system in order to evaluate their requisite propellant mass. The calculations confirmed that atmospheric breathing supersonic retropropulsion has the potential for significant mass savings relative to traditional architectures. Designs with higher oxidizer-to-fuel ratios were more mass efficient. The largest benefit was seen for small inlet area vehicles that leveraged deceleration from a terminal, instantaneous burn over higher thrust throughout the trajectory.

Introduction

- The exploration of Mars has progressed significantly over the last half century due to robotic landers and rovers
  - Landing capabilities of all mission have been based on incremental advances of Viking-heritage technology
  - Large-scale payloads (10+ MT) are beyond the capabilities of Viking-derived technology
- Supersonic retropropulsion (SRP) is a candidate to enable large mass missions
  - Use rocket engines directed in opposition to oncoming airflow to decelerate the entry vehicle
  - Attractive since performance can scale with payload size
  - However, drastically increases mass of vehicles since fuel is stored onboard

- Atmospheric breathing supersonic retropropulsion (AB-SRP) systems can reduce mass constraints on the entry architectures
  - Ingest oxidizer from the surrounding atmosphere and burn with onboard fuel
  - Martian atmosphere is CO_2 so traditional O_2-hydrocarbon combustion is not possible
    - Instead, can burn CO_2 with certain metals such as Mg
- Thrust profile and resulting trajectory are fundamentally changed due to airbreathing propulsion
  - Important to assess how propulsion differences correspond to overall propellant mass differences

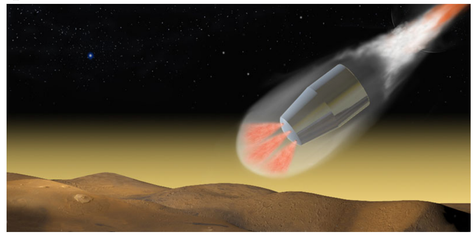

Problem Statement

Can atmospheric breathing supersonic retropropulsion decrease entry vehicle mass by ingesting the oxidizer instead of carrying it onboard?

Propulsion System Overview

Propulsion System Diagram

1) Oxidizer ingestion
2) Oxidizer compression
3) Fuel-oxidizer mixing
4) Combustion
5) Product expansion

A) Fuel tank
B) Vehicle outer mold line

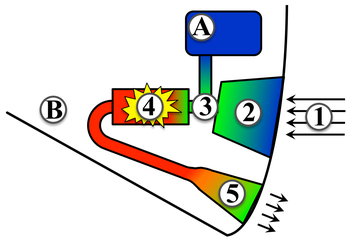

Propulsion System Performance

- Isp = Thrust/(gravity*mass flowrate)
  - Measure of propulsive efficiency
- **Achieve I_{SP} = 140s**
- Airbreathing systems do not use onboard oxidizer
  - Scale I_{SP} by the specific fuel consumption to get $I_{SP,eff}$
  - Better metric to compare to rocket engines
  - **Achieve $I_{SP,eff}$ = 700s**
  - Compare to SRP: I_{SP} = 370s

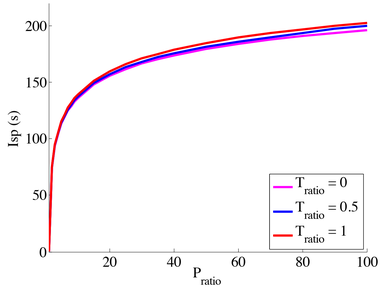

Trajectory Simulation

- 3 DOF, point mass trajectory
- Numerically integrate equations of motion (1) – (4)
- Assumptions:
  - Inlets sweep out of column of atmosphere processing all CO_2 in that column
  - Engines in steady state (5)
  - Exponential atmosphere (6)
  - Constant aerodynamic coefficients, no lift
  - Constant OF = $\dot{m}_{ox}/\dot{m}_{fuel}$
- Vehicle parameters and initial conditions based on literature values of human-scale mission
  - M_{PL}= 40 MT, M_S = 10 MT
  - Start: h = 4600m, v = 555m/s, End: h = 0m, v = 0m/s
- AB-SRP unable to meet 0m/s condition with steady-state thrust
  - Remove final velocity with terminal impulsive burn
  - Oxidizer for terminal burn stored prior to thrust initiation
- Trajectories optimized to land with 0 propellant

$$\dot{v} = -g\sin(\gamma) - \frac{1}{m}\left(\frac{1}{2}\rho v^2 C_D A_{ref}\right) - \frac{T}{m}\cos(\theta) \quad (1)$$

$$\dot{\gamma} = -\frac{g}{v}\cos(\gamma) + \frac{1}{mv}\left(\frac{1}{2}\rho v^2 C_L A_{ref}\right) + \frac{T}{mv}\sin(\theta) \quad (2)$$

$$\dot{h} = v\sin(\gamma) \quad (3)$$

$$\dot{m}_f = \frac{-T}{gI_{SP}(OF+1)} \quad (4)$$

$$T = gI_{SP}\left(\frac{1}{OF}+1\right)\rho v A_{in} \quad (5)$$

$$\rho = \rho_0 e^{-h/H} \quad (6)$$

Results

AB-SRP Configuration Comparison

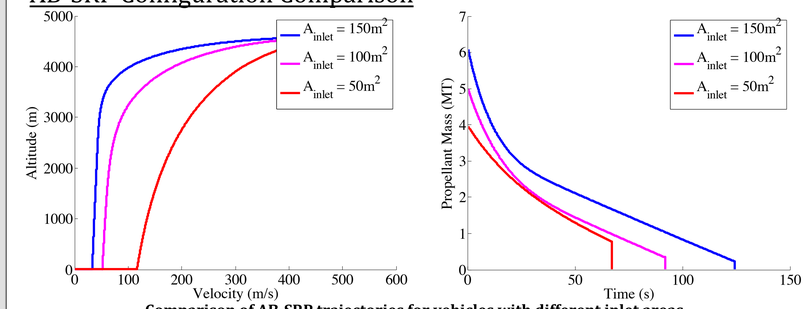

Comparison of AB-SRP trajectories for vehicles with different inlet areas

- AB-SRP vehicles reach pseudo-terminal velocity
  - Dependent on inlet area
- **Smaller inlet: lower total propellant**, larger terminal propellant
  - Vehicle preferences instantaneous burn over continual thrusting
  - Benefit from atmospheric drag and more efficient maneuver
  - Limited by amount of CO_2 capture and acceleration limits

AB-SRP and SRP Comparison

- **AB-SRP has potential to decrease propellant mass**
- Increased benefit for:
  - Large OF - leverage more atmospheric oxidizer
  - Larger I_{SP} – better mass efficiency
- Practical AB-SRP inlet sizes on order of the vehicle frontal area – 80m^2

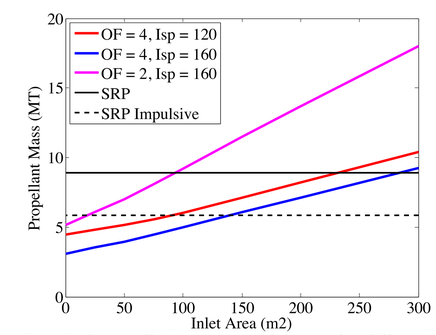

Required propellant mass vs. inlet area for different AB-SRP configurations compared with SRP vehicles

Conclusion

- AB-SRP vehicles reduce propellant mass over SRP vehicles
- Highest benefits seen for large I_{SP} and large oxidizer-to-fuel ratios
- Vehicles with smaller inlets required less propellant – preference terminal burn over continual thrusting
  - Will be reassessed with more accurate estimates of CO_2 capture and acceleration limits
- Architectures exploiting innovative ways to increase oxidizer mass capture will have the most benefit since AB-SRP vehicles are limited by amount of CO_2 ingested

Acknowledgements

This research was funded by the NASA Science and Technology Research Fellowship (NSTRF)

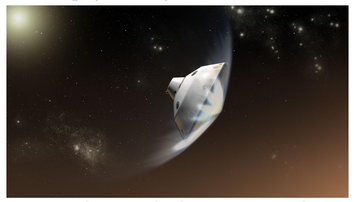

Images: www.nhsgc.sr.unh.edu, mae.virginia.edu, NASA.gov, NASA.gov, The Atlas Group

STANFORD AERONAUTICS & ASTRONAUTICS

DLR

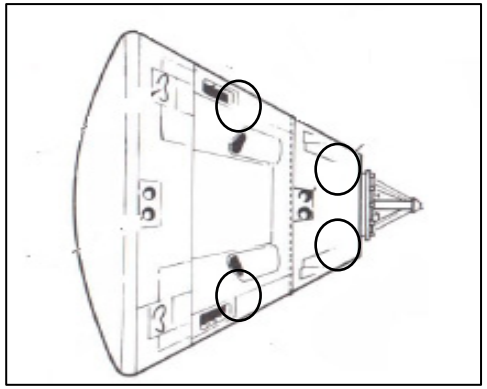

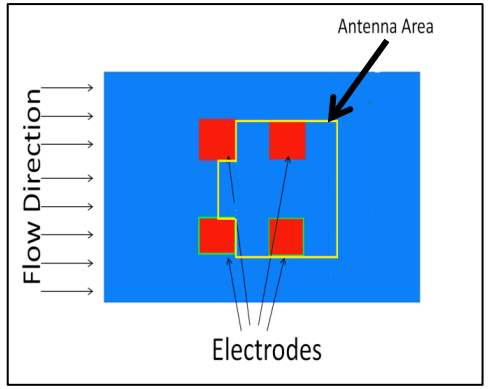

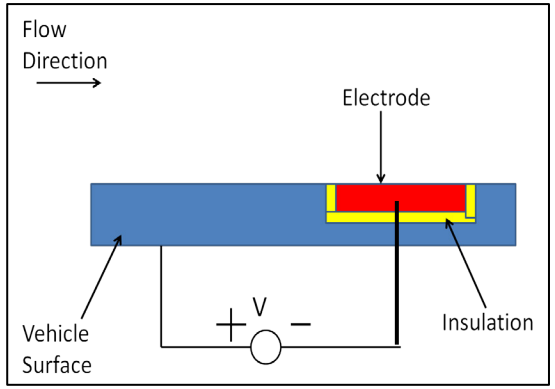

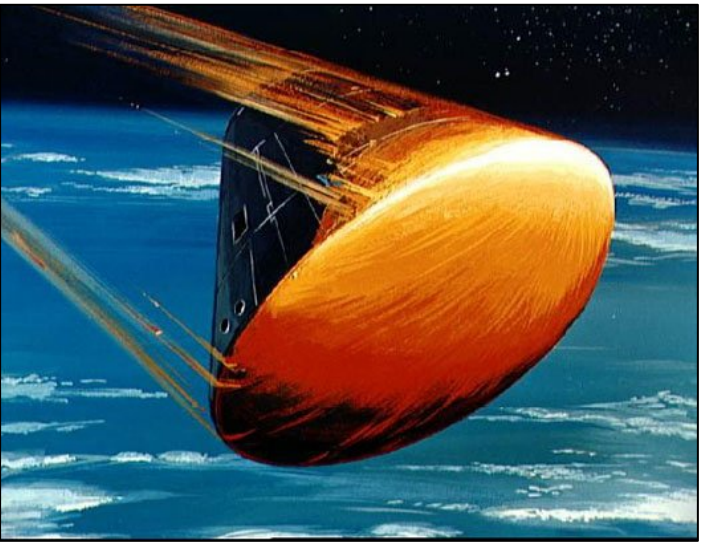

Reentry Blackout Alleviation Through Electrostatic Manipulation of Plasma (#3205)

Siddharth Krishnamoorthy and Sigrid Close

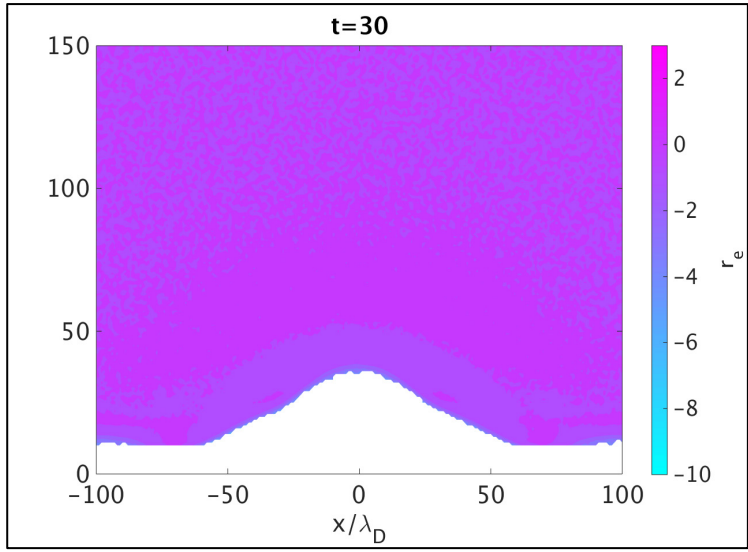

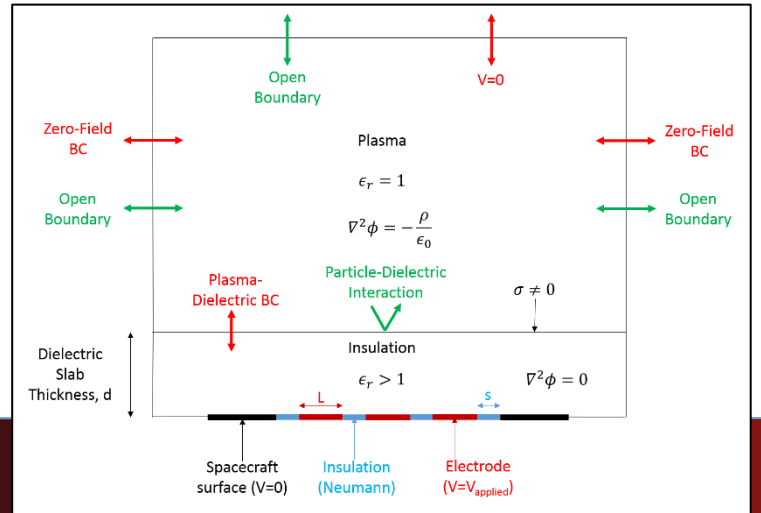

SESS Space Environment and Satellite Systems

Stanford University

Middle East Technical University
Ankara, Turkey

12th International Planetary Probe
June,15-19, Cologne, Germany

ANALYSIS OF HYPERSONIC NON-EQUILIBRIUM REENTRIES WITH NEWTON-GMRES METHOD

Tugba Piskin, Asoc. Prof. Dr. Sinan Eyi
tugba.piskin@metu.edu.tr

ABSTRACT

The aim of this study is to simulate hypersonic flow field around the Apollo Command Module during the reentries of the Earth by using Newton– GMRES method. Modelling high speed hypersonic flow such as re-entries requires consideration of all physical phenomena and that of appropriate numerical modelling. Because of high energetic species, real gas assumption is used to define species state characteristics instead of ideal gas assumptions. Chemical, thermal and vibrational non-equilibrium modelling is the main consideration of this study.

INTRODUCTION

The gravitational accelerations yield reentries with high spend and high energy. With an increasing temperature, the characteristics of flow field change substantially. The dissociation reactions of oxygen starts about 2000K and that of nitrogen starts around 4000K in the reentries of the Earth atmosphere. However, typical maximum temperature during reentries is approximately 25000K. At this temperature, there are ionization and impact reactions in addition to dissociation and exchange reactions. Also, real gas and nonequilibrium effects should be considered for the sake of accuracy of flow solver. There are many models and studies to model thermochemical and physical nonequilibrium with various assumptions

Park's two temperature model [1] is used in this study because of fast interaction between translational-rotational and vibrational- electronic energy modes. To model chemical nonequilibrium different forward rate constants and different equilibrium constant calculations are examined. For the vibrational relaxation, harmonic oscillation assumption and Landau Teller relaxation with modifications are examined [2]. For the thermal nonequilibrium, real and ideal gas assumptions were examined with curve fitted specific heat capacity, entropy and enthalpy values. The simulation of flow field is obtained by using Newton GMRES which is an inexact implementation which satisfy linearity of equation by using GMRES methods. Basically, Newton- GMRES method is an inexact Newton method where norm of the local linear residual is reduced in each step. Also, Newton method is used to evaluate translational and vibrational temperature. Three dimensional Apollo Command Module is chosen as geometry. The aim of this study is to simulate and to compare simulation of the reentries to Earth atmosphere with different assumptions.

METHODS

Mass, momentum, total energy, vibrational energy and species mass conservation equations are written as in form of Euler equation.

$$R(w) = \frac{\partial F\,(w)}{\partial \xi} + \frac{\partial G\,(w)}{\partial \eta} + \frac{\partial H\,(w)}{\partial \zeta} - \hat{S}$$

Newton's method:

$$R^{n+1} = 0 \text{ and } \left(\frac{\partial R}{\partial w}\right)^{n} \Delta w^{n} = -R(w^{n})$$

Inexact Newton's method:

$$\left\| \breve{R}^{n}(\breve{w}) + \left(\frac{\partial \breve{R}}{\partial \breve{w}}\right)^{n} \Delta \breve{w}^{n} \right\| = \mu \left\| \breve{R}^{n}(\breve{w}) \right\|$$

** Approximate solution of exact method
** No need to evaluate Jacobian matrix
** Matrix free
** CPU time efficiency

Chemical Non- Equilibrium

species : N_2, O_2, N, O, NO, N_2^+, O_2^+, N^+, O^+, NO^+ and e (5 and 11 species)

$$k_{f,i}(T_r) = A_i T_f^{\beta_i} e^{-\frac{E_i}{R_u T_r}} \quad , \quad k_{b,i} = \frac{k_{f,i}}{k_{eq,i}}$$

Gibb's free energy minimization: $k_{eq,i} = k_p(T_b)\left(\frac{R_u T_b}{P_{atm}}\right)^{\alpha}$

Park's curve fitted equation: $k_{eq,i} = e^{(c_1 z^{-1} + c_2 + c_3 \ln z + c_4 z + c_5 z^2)}$

Vibrational Non- Equilibrium:

$$E_{v,s} = \frac{R_s \theta_{v,s}}{\left(e^{\frac{\theta_{v,s}}{T_v}} - 1\right)} \qquad \dot{w}_v = \dot{w}_{v-c} + \dot{w}_{v-t} + \dot{w}_{v-v}$$

$\dot{w}_{v-c}$, interactions of vibrational temperature and dissociation reactions
**Park's controlling temperature ($T_c = \sqrt{T_{tr} T_v}$) is used for calculation of the forward reaction rate constant.

$\dot{w}_{v-t}$, modelling energy exchange vibrational energy and translational energy
**Landau-Teller formulation with correction of Park is used for modelling.

$\dot{w}_{v-v}$, energy exchange between molecules having different vibrational energy levels

RESULTS

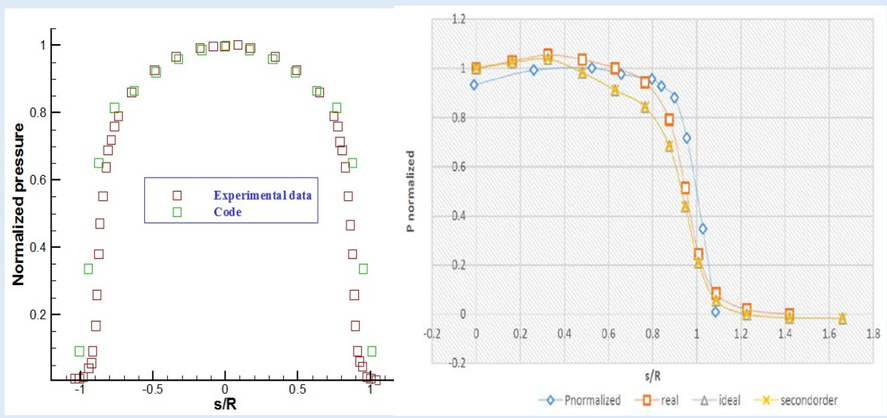

Figure.1 Comparisons of normalized pressure distribution with different assumptions (M=10.18)

Surface pressure around the module are compared with the wind tunnel tests of the small scale version of ACM. The various results for normalized pressure at stagnation line are given in Murray study [3]. These results are obtained from Bertin's [4] and Marvin's [3] wind tunnel experiments.

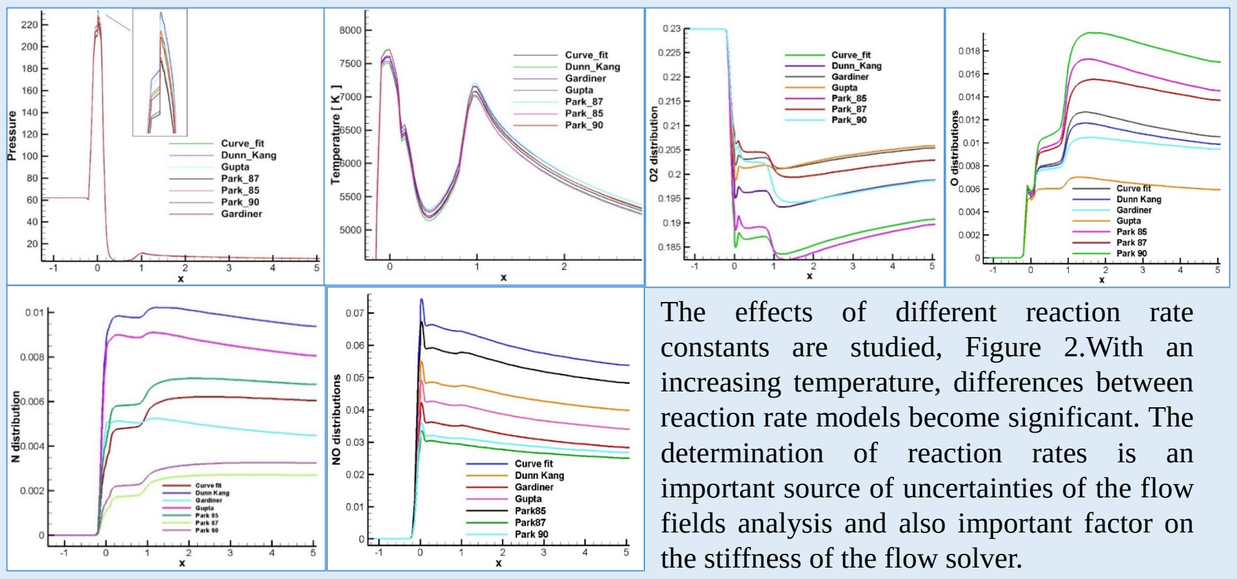

The effects of different reaction rate constants are studied, Figure 2.With an increasing temperature, differences between reaction rate models become significant. The determination of reaction rates is an important source of uncertainties of the flow fields analysis and also important factor on the stiffness of the flow solver.

Figure.2 Comparisons of effects of different constants to calculate forward reaction rates on flow variables

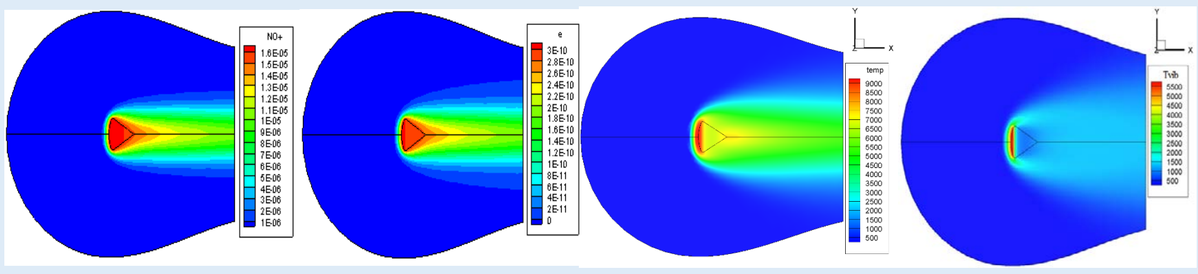

Figure.3 NO+ and electron countours as well as translational and vibrational temperature countours.

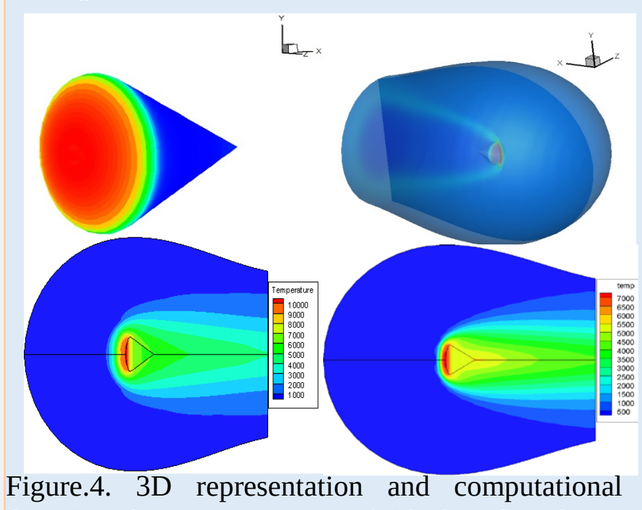

Figure.4. 3D representation and computational domain; also, comparisons of ideal and real gas assumptions in terms of T

In Figure 3, ionized species and electron mass fractions can be seen. Moreover, translational and vibrational temperature countours are given. Vibrational temperature countours are similar to translational temperature; however, the peak values are different, and vibrational interactions continue at the wake of geometry. The whole geometry and computational domain are shown in Figure4. Also, in this figure, temperature values from ideal (left) and real (right) gas assumptions are given. In the blunt bodies, shock standoff distance is reduced due to real gas effects [1]. Also, there are differences in surface heating rates, shock characteristics and flow compositions.

REFERENCES

[1] Park, C. (1990). Nonequilibrium Hypersonic Aerothermodynamics. John Wiley & Sons
[2] Vincenti, W. G., & Kruger, C. H. (1967). Introduction to Physical Gas Dynamics. New York: Wiley
[3] Murray, A., (1999).Aeroheating Analysis for Planetary Re-Entry Vehicles. ITT Industries.
[4] Bertin, J.J. The Effect of Protuberances, Cavities, and Angle of Attack on the Wind Tunnel Pressure and Heat Transfer Distribution for the Apollo Command Module. NASA TM. (1966)

ACKNOWLEDGEMENTS

This research is supported by The Scientific and Technological Research Council of Turkey (TUBITAK).

Molecular Simulation of Heat Shields

Savio J. Poovathingal[1], Eric C. Stern[2], Thomas E. Schwartzentruber, Graham V. Candler. [1]poova002@umn.edu, [2]eric.c.stern@nasa.gov

Molecular simulations are used to understand and model detailed physical processes occurring in both, porous and non-porous ablating heat shields. The microstructural surface of a real heat shield sample is obtained through 3D reconstruction using X-ray micro tomography and then used in the Direct Simulation Monte Carlo (DSMC) solver Molecular Gas Dynamics Simulator [1] to perform molecular simulations.

The goal of such molecular modeling is to understand ablation physics at the most fundamental level, in order to reduce uncertainty margins on heat shield and to design better thermal protection systems for future hypersonic missions.

X-ray computed tomography and surface grid for simulations

X-ray computed tomography (X-ray CT) is used to generate a 3D image of the inside of the object from a large series of two-dimensional radiographic images taken around a single axis of rotation [2].

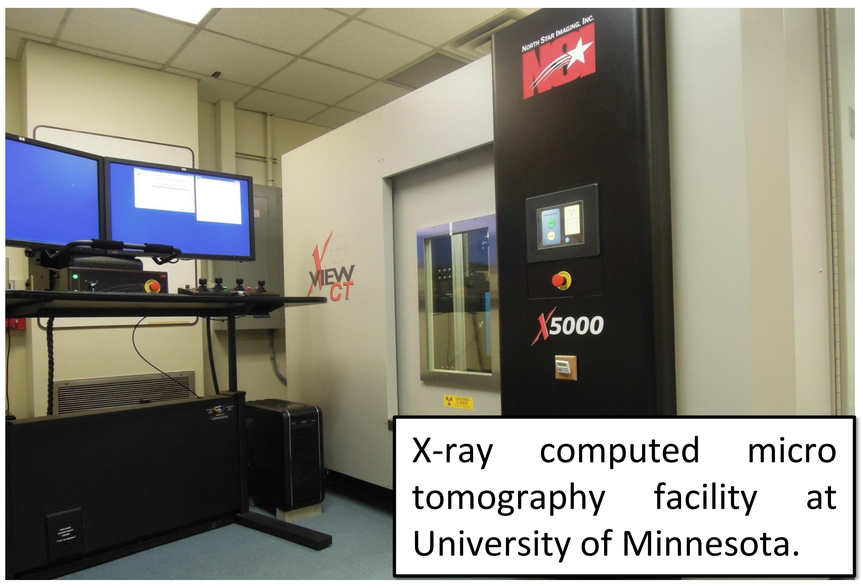

X-ray computed micro tomography facility at University of Minnesota.

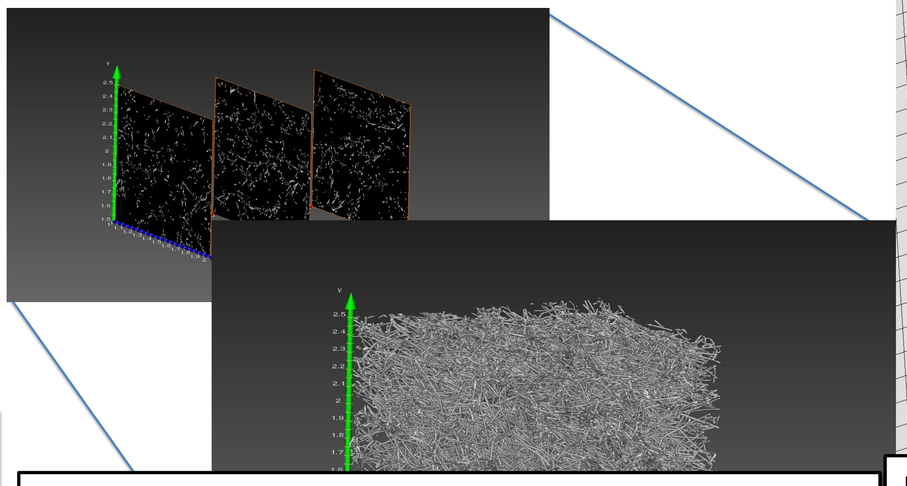

Illustration of the reconstruction of a 3D surface from the 2D slices from tomography.

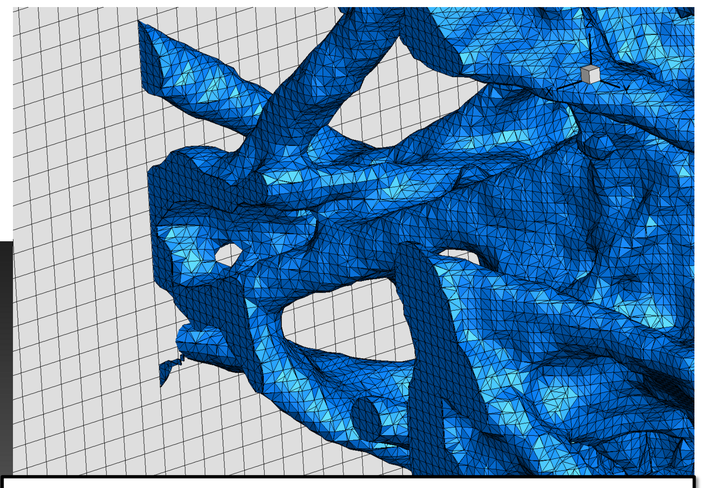

Demonstration of the robust cut-cell algorithm [3] applied to a porous microstructure obtained from microtomography.

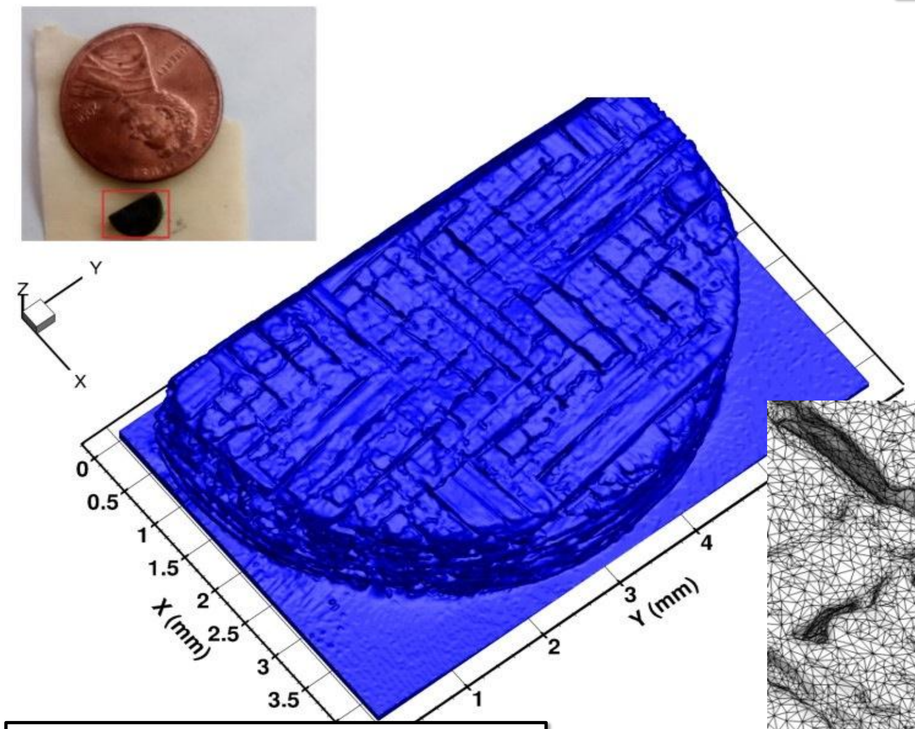

3D reconstructed surface of a Carbon-Carbon composite. The sample is shown in the inset.

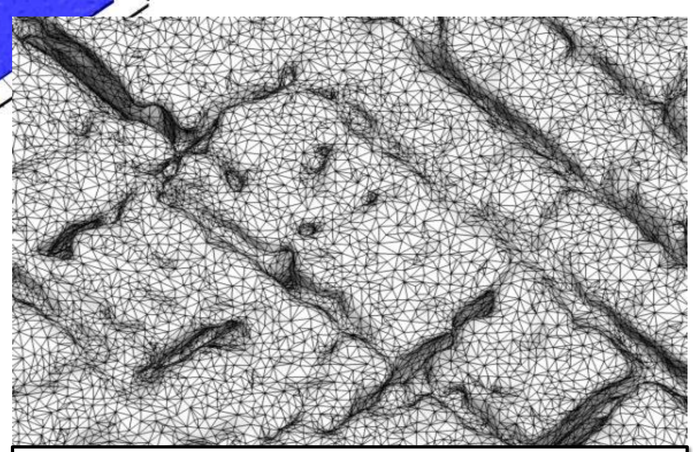

Surface grid of 5 million triangles[3] on a real C-C composite.

Atomistic analysis of carbon based heat shields

Atomistic analysis provides detailed data on the chemical reactions occurring on a carbon surface. The analysis is aided through experiments [4] and SEM images. The molecular beam data is used as input for DSMC boundary conditions to propose oxidation model for full vehicle CFD simulations.

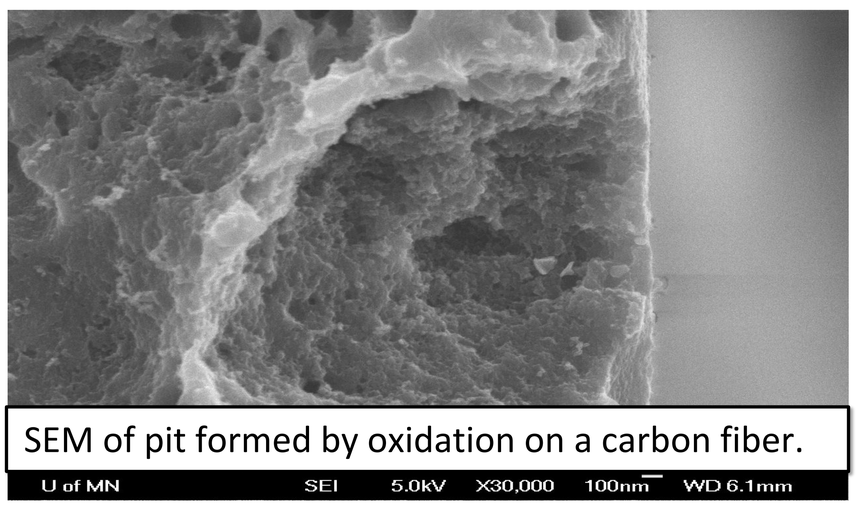

SEM of pit formed by oxidation on a carbon fiber.

Flow study at the micro scale using DSMC

DSMC simulations are performed using the real surface and reaction chemistry data from beam experiments.

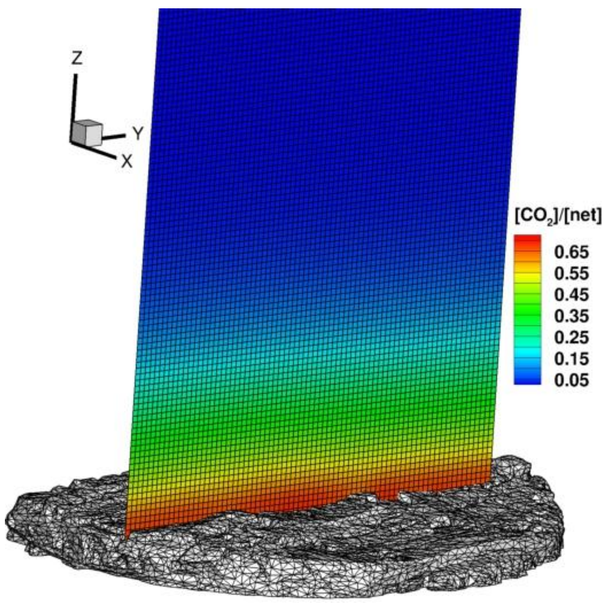

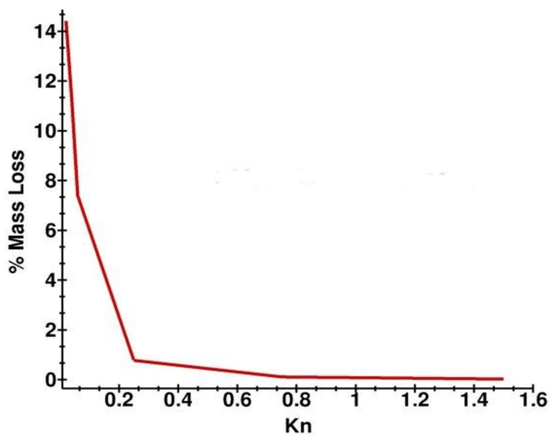

DSMC simulations of flow over the real C-C composite. CO_2 production is observed due to gas phase reactions [5] within the gaps of the fibers despite CO being the dominant product at the atomistic scale. Higher mass loss is observed due to such gas-phase reactions.

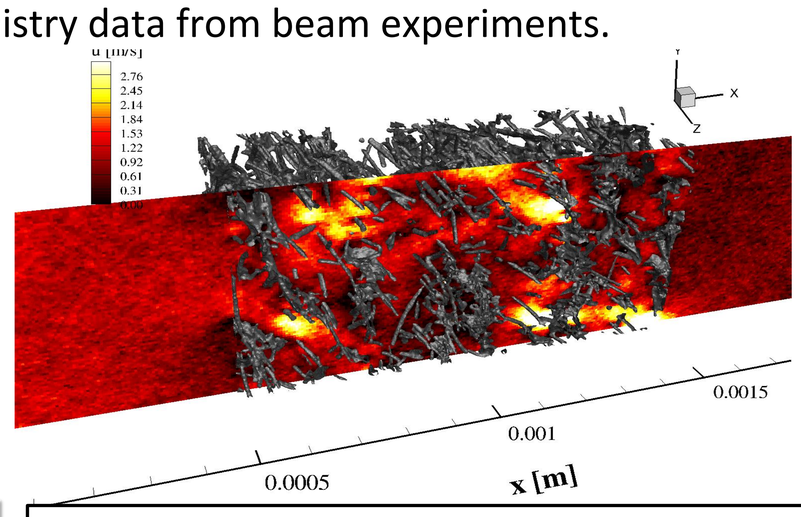

U-velocity contours from a DSMC Simulation of pressure driven flow through FiberForm. Surface generated using data from micro-tomography contains over 6 million triangular surface elements.

References

1)Nompelis I., Schwartzentruber T.E., AIAA 2013-1204.
2)Stern E. et. al. , AIAA 2015-1450.
3)Zhang C., Schwartzentruber T.E., Computers and Fluids, Vol. 69, 2012.
4)Murray et. al., J. Phys. Chem C., Web Publication Mar 26 2015.
5)Poovathingal et. al., AIAA 2015-1449.

Acknowledgments

The authors would like to thank Dr. Brian Bagley for X-ray computed tomography, Vanessa J. Murray and Prof. Tim Minton for the molecular beam data and Prof. Erica Corral for the C-C composite sample. Dr. Stern's was supported through a NASA Space Technology Research Fellowship.

IPPW2015-3209

CLOSED MOLDING OF CONFORMAL ABLATIVE THERMAL PROTECTION SYSTEM MATERIAL

A. T. Sidor[1*] and R. D. Braun[2*], [1]Graduate Research Assistant, adam.sidor@gatech.edu, [2]David and Andrew Lewis Professor of Space Technology, robert.braun@ae.gatech.edu, *Space Systems Design Lab, Georgia Institute of Technology, Atlanta, GA 30332.

Introduction and Background

Introduction

Ablative thermal protection systems (TPS) have been used almost exclusively for planetary probes to date because of their high heat rate and heat load capabilities [1]. Manufacturing and installing these TPS materials can present significant engineering and processing challenges due to limited tile size (resulting in heat shields with large part counts) and/or complex, costly fabrication processes. Conformal ablators, C-PICA and C-SIRCA, show promise in alleviating these difficulties by utilizing a flexible fibrous substrate, which results in a higher stain-to-failure than traditional rigid ablative TPS [2]. The present work aims to select a closed mold manufacturing process for conformal ablators with the goal of facilitating larger tile sizes and reducing labor, cost and waste.

Conformal Ablators

Lightweight ceramics ablators (LCAs), including PICA and SIRCA, utilize porous, fibrous ceramic or carbon substrates impregnated with a polymer resin filler. These ablators have improved mass efficiency and superior strength over traditional ablators, which consist of short disconnected fibers and/or organic filler in a polymeric mixture [3,4].

The rigid carbon preform of PICA contributes to processing and integration challenges:

- Material waste due to post-processing / machining
- Limited tile size / high part count
- Strain isolation pad, SIP, necessary for bonding to aeroshell structure

Conformal ablators replace the rigid substrate with a flexible felt – the resulting material has a higher strain-to-failure and can be manufactured and integrated more easily.

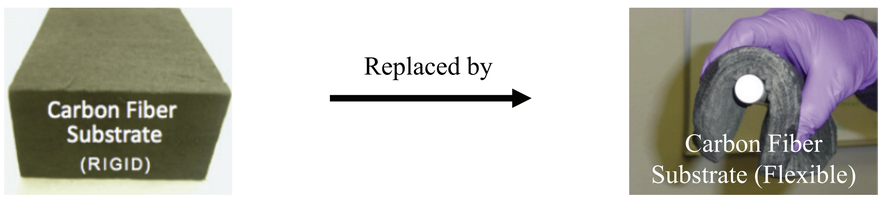

Closed Molding

Closed molding utilizes sealed, rather than open, tooling to improve resin infiltration and control volatile compounds. Established techniques exist for fiber-reinforced plastics (FRP).

- Tooling can be rigid and/or flexible.
- An applied pressure differential between the inside and the outside of the tool enables flow of resin and evacuation of volatiles during curing.
- Some processes utilize fiber preforms pre-impregnated with resin (prepreg); other processes (i.e. resin infusion processes) use a dry preform with resin injected from an external reservoir.

Closed molding concept (adapted from [2]):

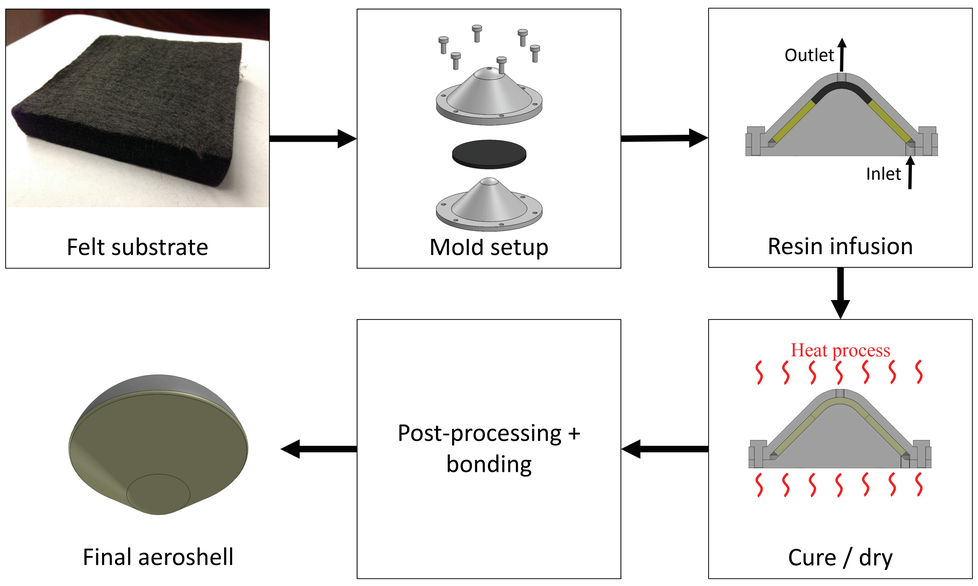

Potential advantages to TPS manufacturing [6,7]:

- Near net-shape molding (and thus reduced waste)
- High levels of controllability and repeatability
- Reduced labor
- Larger part sizes

Acknowledgements

This work is funded through a NASA Space Technology Research Fellowship (Grant #NNX14AL53H). The authors would also like to thank Robin Beck of NASA Ames Research Center for her guidance on this work.

References

[1] Laub, B., and Venkatapathy, E. (2003) IPPW-1. [2] Beck, R. A. S. et al. (2012) IPPW-9. [3] Tran, H. K. (1994) NASA TM-108798. [4] Rasky, D. J., and Tran, H. K. (1999) Acta astronautica, vol. 45, 347–355. [5] Venkatapathy, E. (2013) IPPW-10. [6] Lewit, S., and Jakubowski, J. (1997) 42nd SAMPE Symposium, 1173–1187. [7] Strong, A. B. (2008) Fundamentals of Composites Manufacturing, 2nd edition.

Methodology and Results

Evaluation of Closed Mold Processes

Closed mold process were narrowed down to resin infusion processes, exclusively, because of similarity/applicability to TPS fabrication. Evaluation based on qualitative criteria (with scale in parentheses):

- Cost (low / medium / high)
- Process time (short / medium / long)
- Amount of labor (low / medium / high)
- Surface finish quality on both the inner mold line (IML) and outer mold line (OML) (good / fair / poor)
- Maximum typical operating pressure (low / medium / high) [Note: lower pressure results in relaxed equipment requirements]

To compare processes, criteria are assigned numerical scores between 1 (best) and 3 (worst), e.g. long process time = 3. Both surface finish categories are weighted by 50% so as not to have an overly large influence on the final score. Cost and labor are weighted by 150% indicating their relative importance to the goals of the research. Resulting category scores are summed to produce the combined score (with a lower score corresponding to a better option).

Process Selection

Processes were evaluated based on the above criteria. Selected results are presented in the table below. Vacuum Infusion Processing (VIP) was selected as the candidate process. Both the scoring process and other indicators point to VIP as the appropriate selection. VIP is suited to low viscosity resins. Also, low operating pressures may allow the use of non-metallic tooling, simplifying mold design.

Process	Cost	Process Time	Labor	Surface Finish – IML	Surface Finish – OML	Max. Pressure	Combined Score*
Resin Transfer Molding	High	Short	Low†	Good	Good	Medium	10
Vacuum Infusion Processing	Low	Medium	Low†	Fair	Fair	Low	7.5

*Lower scores are better. †Fully automated processes are possible albeit after substantial development.

Preliminary Process Concept

VIP encompasses a family of similar processes. A VIP mold is illustrated below for a notional 1m^2 tile. The design is conceptual only.

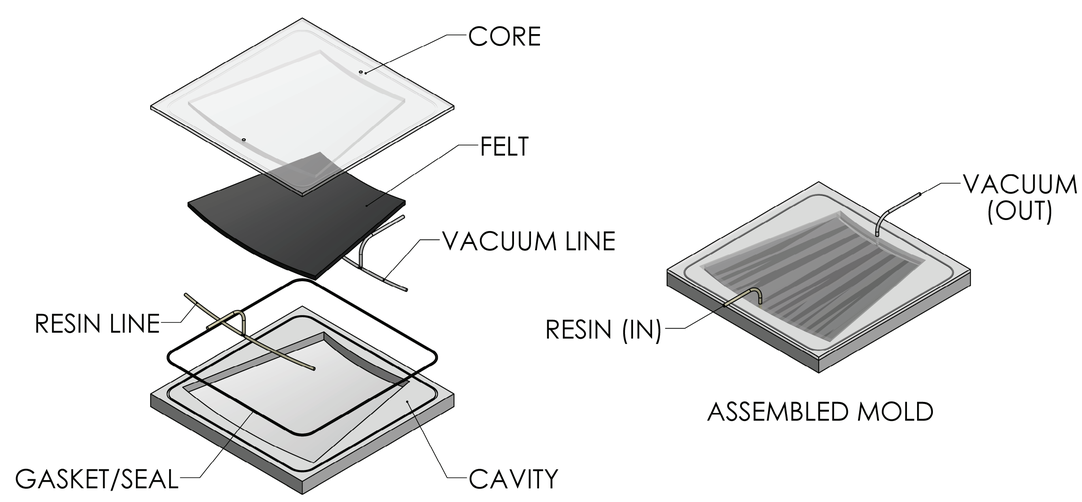

Important process parameters to control [7]

1. Resin viscosity
2. Pressure differential
3. Injection ports (number and locations)
4. Fiber substrate compaction (high compaction reduces thermal performance)

Conclusion

Conclusion and Future Work

Manufacturing conformal ablators using closed molding has the potential to reduce processing waste and labor at relatively low cost. The low strain-to-failure of conformal ablators can also simplify assembly and integration to the aeroshell structure. These advancements reduce burden on project schedule and budget. Vacuum Infusion Processing (VIP) was selected as a candidate manufacturing process for conformal ablators. A preliminary concept of the infusion process was outlined. In future work, these processes will be implemented in the laboratory on a small scale. Once successfully demonstrated, the process will be scaled up to produce larger TPS segments (with a goal of 1m^2 tiles).

Overview of the Gen-2 3.7m HIAD Static Load Test Series

G.T. Swanson[1] (g.swanson@nasa.gov), C.D. Kazemba[2], R.K. Johnson[3], S.J. Hughes[3], A.M. Calomino[3], F.M. Cheatwood[3], A.M. Cassell[4], B. Gilles[5], P. Anderson[5], A. Lowery[5]

[1]ERC Inc @ NASA ARC, [2]STC Corp @ NASA ARC, [3]NASA LaRC, [4]NASA ARC, [5]Airborne Systems

Why Static Load Testing?

- Demonstrate structure maintains acceptable shape under load
- Demonstrate structure robustness to max loading conditions
- Experiment with different layouts and inflation conditions to determine the acceptable lowest mass inflation state
- Inexpensive compared to alternative structural tests

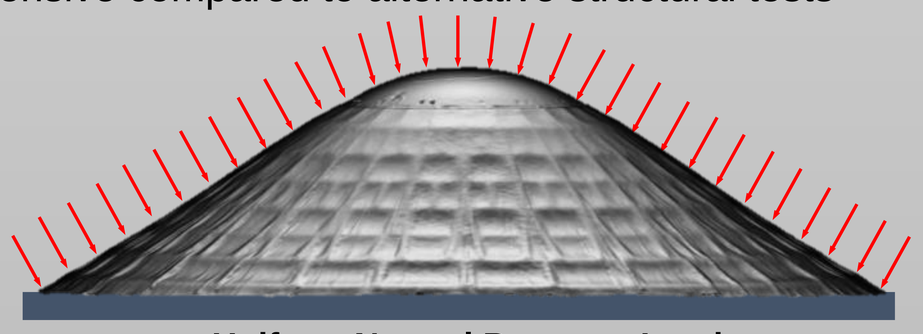

Uniform Normal Pressure Load

Static Load Test Setup

- Vacuum Fixture (Tub)
- Hydraulic Ram & Cross Member
- Slip Sheet & Vacuum bag
- 50,000lb Loadcell & Manometer
- Industrial Vacuum

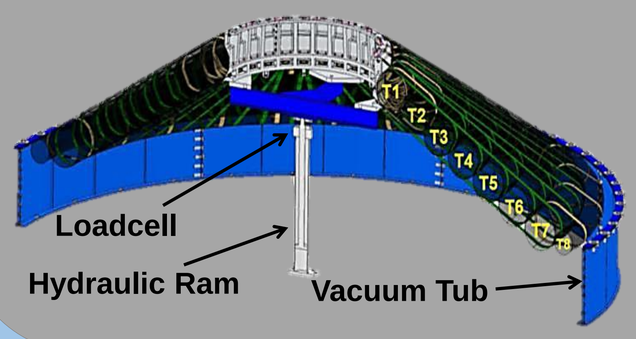

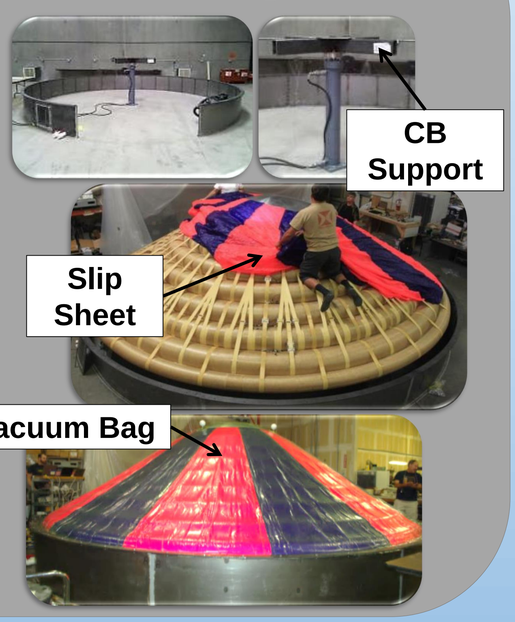

Gen-2 HIAD Test Article

3.7 meters

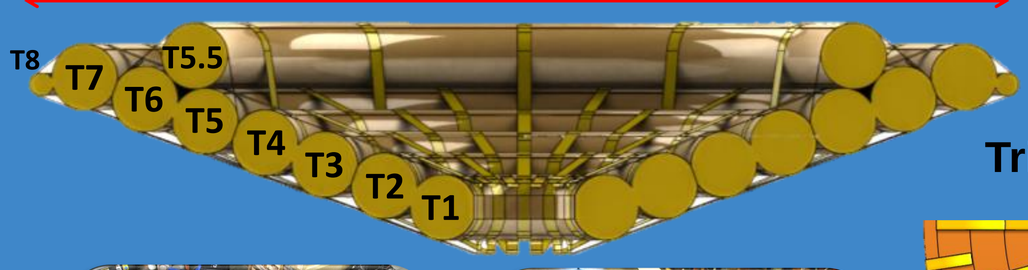

Material: Zylon
Cone-Angle: 70 Deg
Coating: RTV
Liner: Urethane
Tri-Torus: T5.5 (removable)

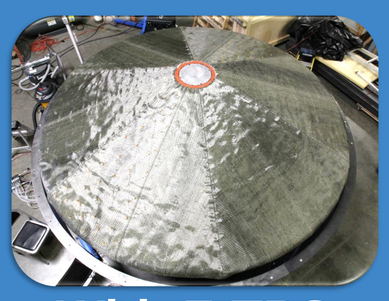

With F-TPS

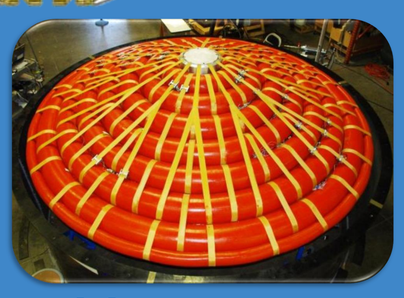

Without F-TPS

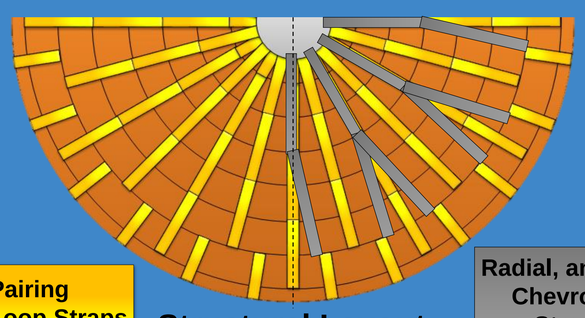

Structural Layout

Instrumentation

Laser Scanner

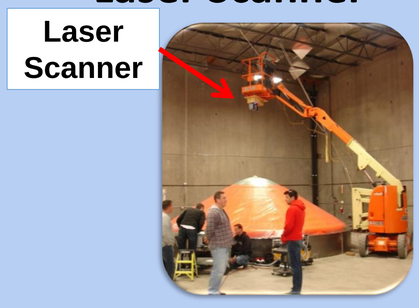

Strap Loadcells

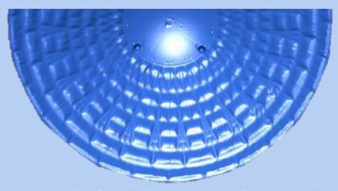

Matlab Plots using 3D Point Cloud Files

Example Test Results

Inflation Pressure Comparison

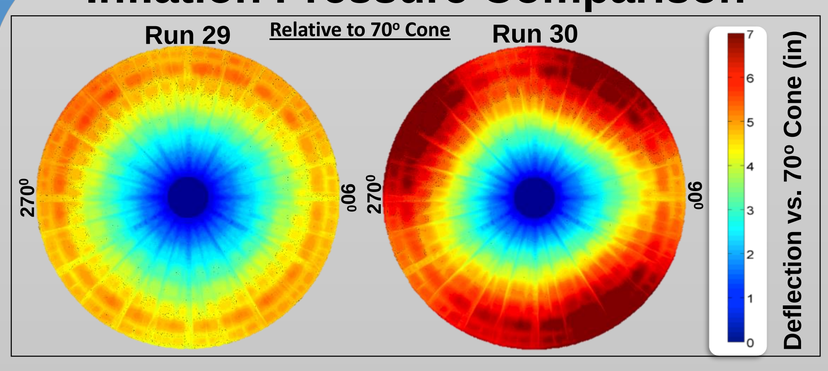

- **12 psi:** Uniform Deflection Under 10,000lb Load (Run 29)
- **10 psi:** Aersohell Begins Asymmetric Deflection (Run 30)

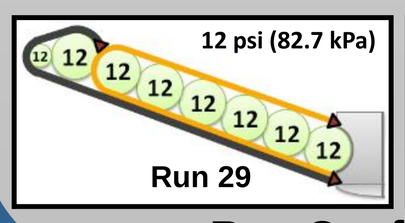

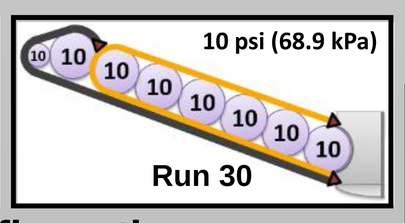

Run Configuration

Chevron Webbing Termination

- **Centerbody Chevron Termination:** Slight Deflection Reduction, Pairing Loop Load Reduction (Run 29 vs 24)

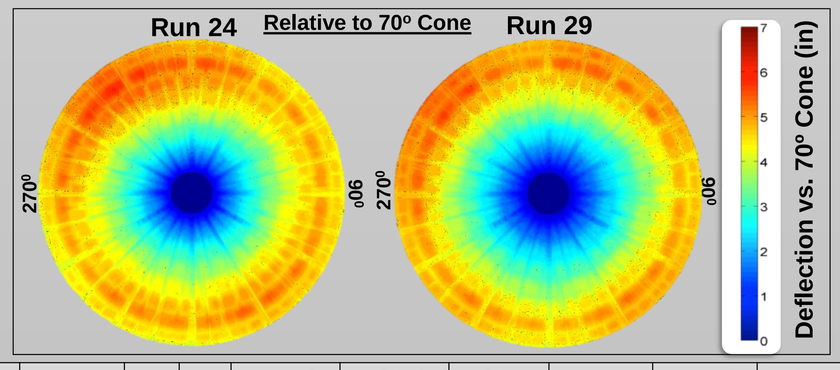

10,000 lbs	R	CF	T1/T2		T2/T3		T3/T4		T4/T5		T5/T6		T6/T7	
Run			Fwd	Aft	Fwd	Aft	Fwd	Aft	Fwd	Aft	Fwd	Aft	Fwd	Aft
Run 24	458	210	164	170	173	173	137	2	-12	-25	-58	78	-1	1
Run 29	411	186	126	127	129	99	111	39	-27	-34	-55	23	-5	23
Diff (lbs)	**-46**	**-24**	**-38**	**-43**	**-44**	**-75**	**-26**	**37**	**-15**	**-8**	**4**	**-54**	**-4**	**23**
%Change	**-10.1**	**-11.5**	**-23.2**	**-25.5**	**-25.5**	**-43.1**	**-18.9**	**-**	**-**	**-**	**-**	**-69.7**	**-**	**-**

Tri-Torus vs. Baseline Configuration

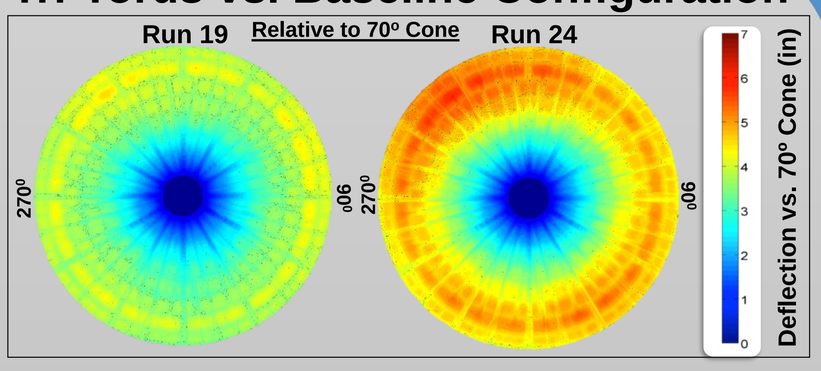

- **With Tri-Torus:** Less Deflection by ~2in (Run 19)
- **Baseline (No Tri-Torus):** Less Shoulder Stiffness (Run 24)

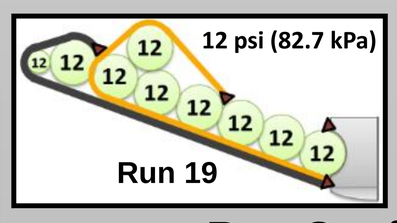

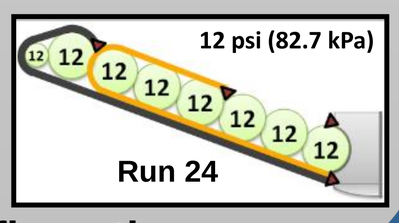

Run Configuration

Conclusions and Future Work

- Aeroshell performs well at 10,000lbs (~4,500kg) of load with an inflation pressure of 12 psi (82.7 kPa)
- Alternate chevron termination reduces load In inflatable structure
- Tri-Torus increases rigidity of structure, but decreases volume & mass efficiency

- Develop and test 15m class Gen-2 HIAD aeroshell
- Perform pack and deploy testing on Gen-2 HIAD aeroshell
- Conduct greater Zylon environmental testing to fully characterize current system and document limitations

Static Load Test Team

Laser Scan 3D Point Cloud

Hazard Assessment of Thruster Plume Induced Surface Alteration for the InSight Mission

Devin Kipp, Rob Grover, and Mike Lisano
Jet Propulsion Laboratory, California Institute of Technology

Mars Phoenix Experience

The InSight lander is nearly identical to the Phoenix lander which landed successfully in 2008. Soil beneath Phoenix' thrusters eroded down to shallow layer of competent subsurface ice. Such an ice layer is not present within InSight landing region, leading to concern over the potential of increased significant surface alteration during touchdown.

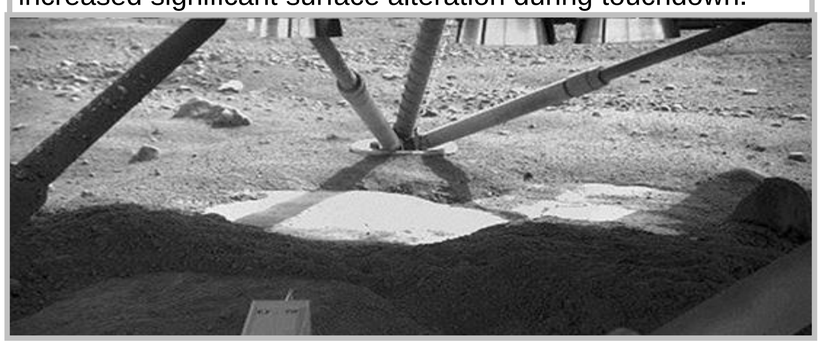

InSight Surface Configuration

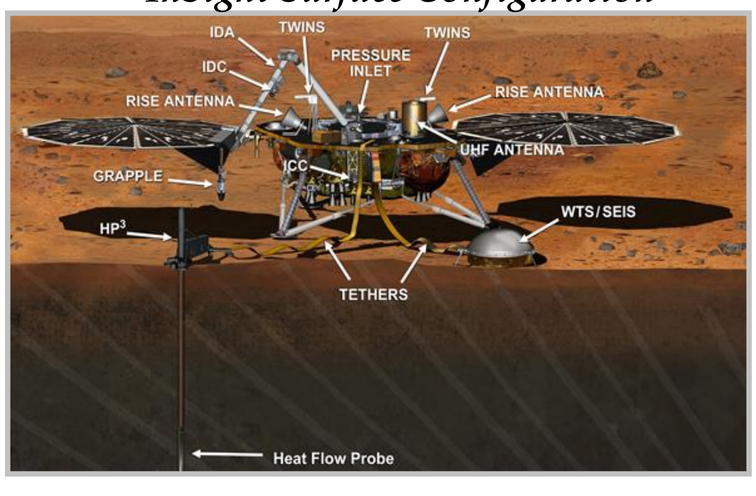

Background

Abstract

Near-surface use of retrograde thrusters when landing on an unprepared surface will necessarily result in modification of local topography near the landing site. While the physical mechanisms governing erosion are generally understood for jet impingement on soil, the use of pulse-modulated thrusters introduces complex erosional mechanisms that are poorly understood. Under the constraints of the InSight mission it was not practical to develop and validate a rigorous method to accurately model pulse-modulated thruster interactions with the surface. Instead, focus was placed on pursuit of an approximate method to enable bounding risk assessment. An approach based on conservation principles, as described in this poster, was used to characterize the potential for site alteration during InSight landing. Associated mission risks were deemed to be acceptably low.

Surface Alteration Testing (1973)

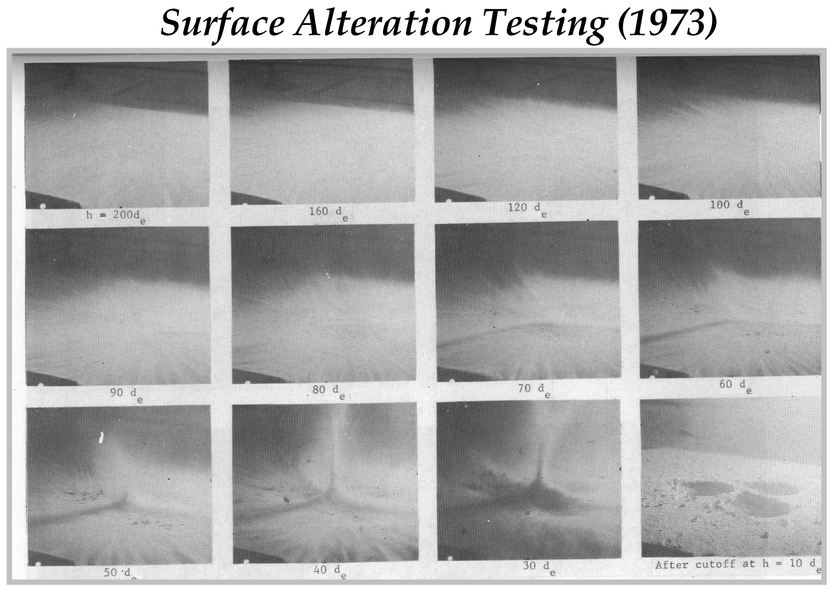

Erosional Mechanisms

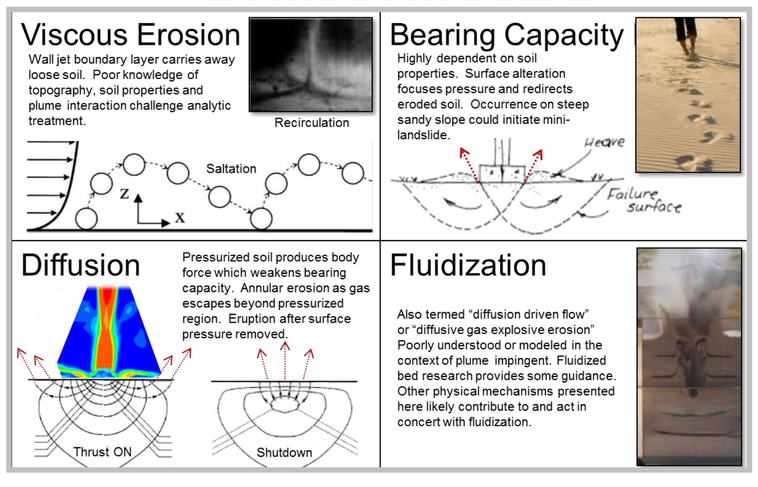

Method

1- A Simple Model

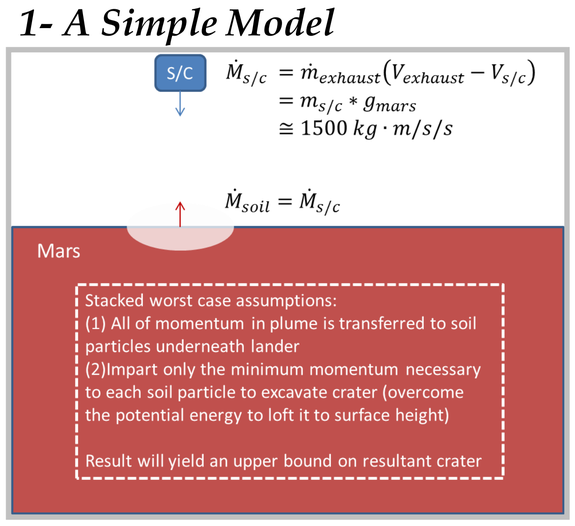

A simplistic approach was leveraged to approximate and bound the potential for site alteration during InSight landing and the associated mission risks:

- ➢1-Formulate a simple model based on momentum conservation
- ➢2-Develop equations to calculate total momentum transfer necessary to excavate a given crater
- ➢3- Apply the method to heritage data for point validation
- ➢4- Generate bounding input parameters to assess InSight site alteration

2- Momentum Transfer to Excavate Craters

- Momentum transfer to a given particle must provide enough velocity to reach the height of the crater rim, (derive critical velocity from KE → PE):
  - $M_{critical} = \{V_{critical}\} * \{\text{mass of particle}\}$
  - $M_{critical} = \{\text{sqrt}(2gh)\} * \{m\}$

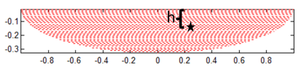

- Assume any particles lofted to this height magically disappear…
- Assuming an axisymmetric crater with a defined depth-vs-diameter profile:

$$M_{required} = \int_{h_{min}}^{0} \{V_{critical}(h)\} * \{mass\ of\ particles\ at\ depth = h\}$$
$$= \int_{h_{min}}^{0} \{\sqrt{2g_m h}\} * \{\rho A(h) dh\}$$
$$= \{\sqrt{2g_m}\} * \{\rho(\pi r^2)\} \int_{h_{min}}^{0} \{r(h)^2 \sqrt{h}\, dh\}$$

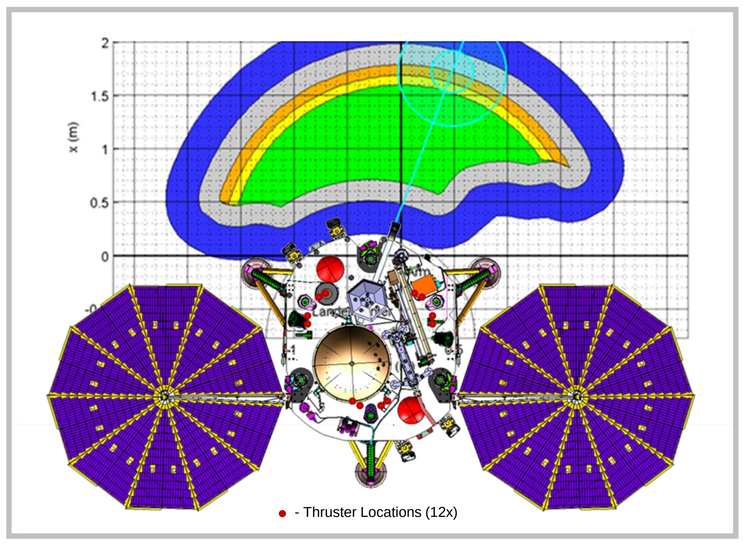

Landed Configuration and Deployment Zone

3- Point Validation

Method was applied to compare momentum available in thruster plumes against the momentum transfer required to excavate an observed crater. All case studies yielded momentum transfer efficiencies of <50%.

	Momentum Transfer Efficiency	Comments
PHX Flight	28% / 1s	Likely mitigated by subsurface ice
Viking Flight	<1% / 1s	Mitigated by design (showerhead nozzle)
MSL Flight	<1% / 1s	Mitigated by design (nozzle height), bedrock
PHX Test	10%-30%	Subscale pulsed testing by Mehta, et al across range of particle sizes
Viking Analysis	< 42% / 1s	Based on max erosion estimate for original baseline bell nozzles
Morpheus Test	unknown	Method predicts entire simulant bed (1750kg) eroded within 0.12 seconds

4 -Bounding Risk Assessment

A small set of assumptions are necessary to enable bounding assessment:

- ➢Soil Bulk Density
- ➢Crater depth-vs-diameter profile
- ➢Momentum Transfer Efficiency (Erosion Efficiency)
- ➢Erosion Onset Altitude (Erosion Duration)
- ➢Lander Tolerance (~40cm depth at footpad)

With conservative assumptions for the above, this analysis predicts InSight has robust margins of 200% - 500% against defined failure thresholds.

Conclusions

- ➢Analysis technique developed based on conservation principles with the aim of bounding the level of flight risk posed by plume-induced site alteration.
  - ➢Not a rigorous solution nor an accurate model of the interaction physics
  - ➢Technique shown to successfully bound prior flight and test experience
  - ➢Technique predicts InSight has healthy margins against failure scenarios
- ➢Simplicity of the approach lends itself to application for bounding a wide range of thrust impingement problems regardless of planetary body of lander architecture

Acknowledgements

➢The authors would like to acknowledge the contributions of the InSight Site Alteration Working Group, specifically:

- ➢Jordi Paredes, JPL
- ➢Manish Mehta, NASA MSFC
- ➢Jeff Vizcaino, NASA MSFC

Contact Info

For more information, contact:

Devin Kipp
Jet Propulsion Laboratory
California Institute of Technology

Email: Devin.M.Kipp@jpl.nasa.gov

National Aeronautics and Space Administration

Jet Propulsion Laboratory
California Institute of Technology
Pasadena, California

www.nasa.gov

HIGH ENTHALPY FLOW DIAGNOSTICS

S. Löhle, M. Eberhart, H. Fulge, T. Hermann, T. Marynowski, A. Meindl, F. Zander

The High Enthalpy Flow Diagnostics Group at the Institute of Space Systems of the University of Stuttgart focuses on development and application of diagnostic methods to characterise high-enthalpy flows as occuring during re-entry, supersonic combustion, and rocket flights. The measured data improves the understanding of fluid-structure interaction and the application in real flight provides validation of the testing.

PHOTOGRAMMETRY

Time resolved measurement of the 3D surface of samples during test using DSLR cameras [1].

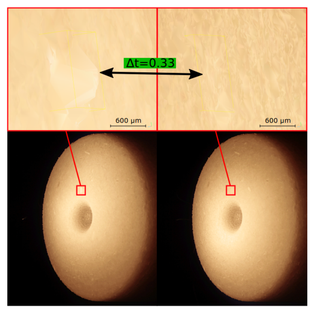

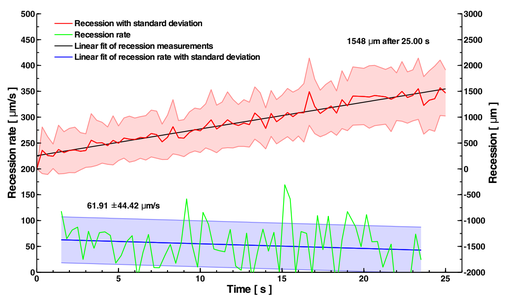

INVERSE METHODS

Transient heat flux measurements using laser calibration for system identification [2].

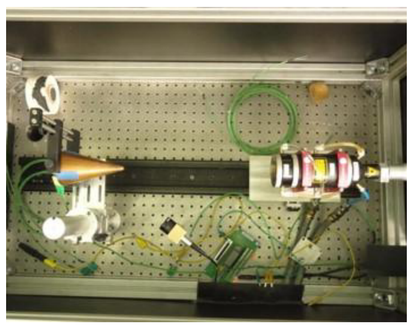

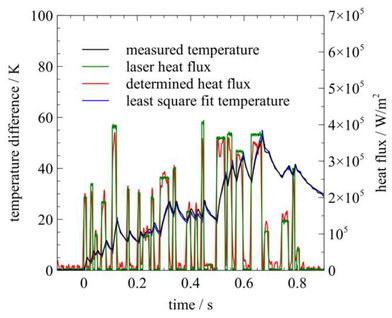

ENTHALPY PROBE

Measurement of the local mass-specific enthalpy using mass injection [3].

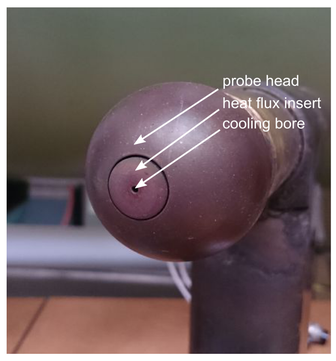

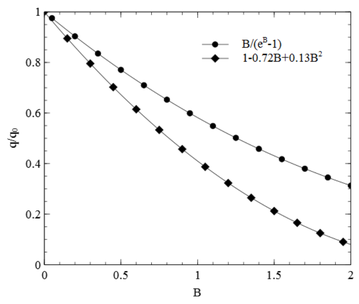

Diode Laser Absorption (DLAS) [4]

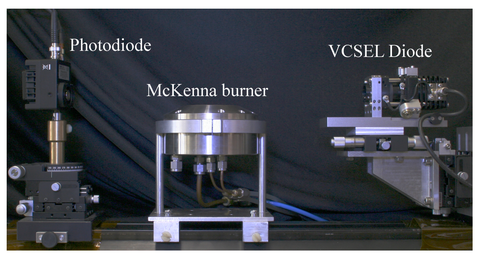

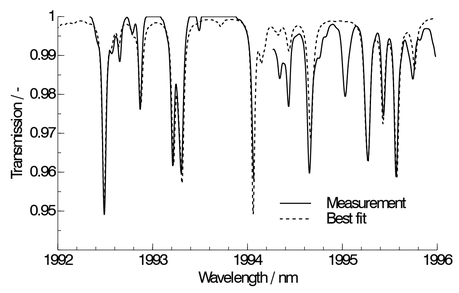

Two-Photon Polarisation Spectroscopy (TIPS)

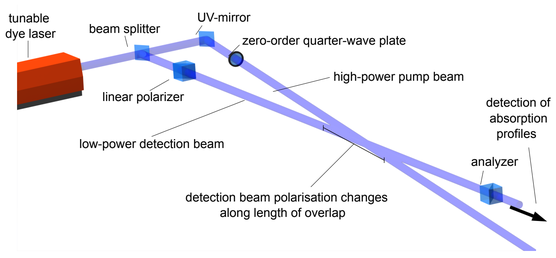

Laser-induced Fluorescence (LIF) [5]

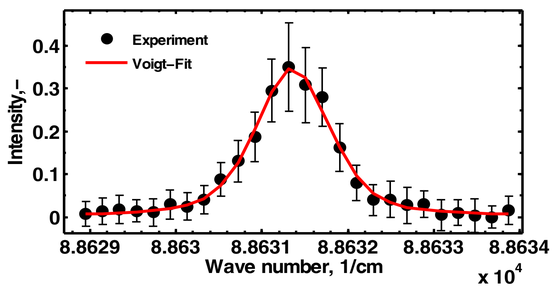

LASER DIAGNOSTICS

Number density, temperature, and velocity measurements through diode laser absorption, polarisation and laser-induced fluorescence spectroscopy [4,5].

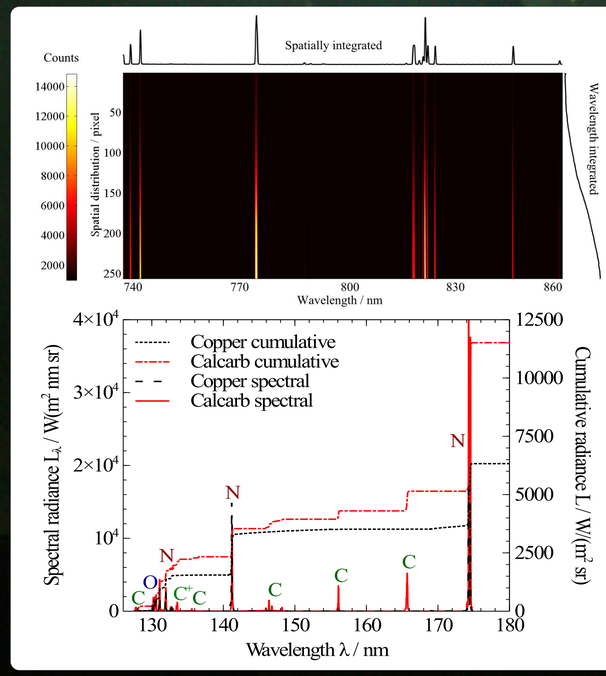

EMISSION SPECTROSCOPY

Analysis of aerothermodynamics and chemistry through measurements of VUV to NIR spectra [6].

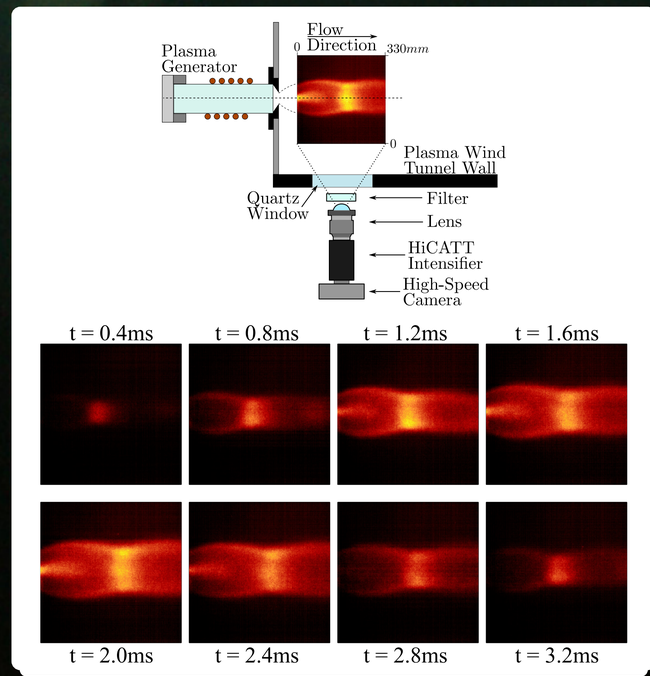

HIGH SPEED IMAGING

Analysis of temporal variations in the steady state flows from high speed imaging data [7].

WADIS

Sounding rocket experiment to measure atomic oxygen using solid electrolyte sensors [8].

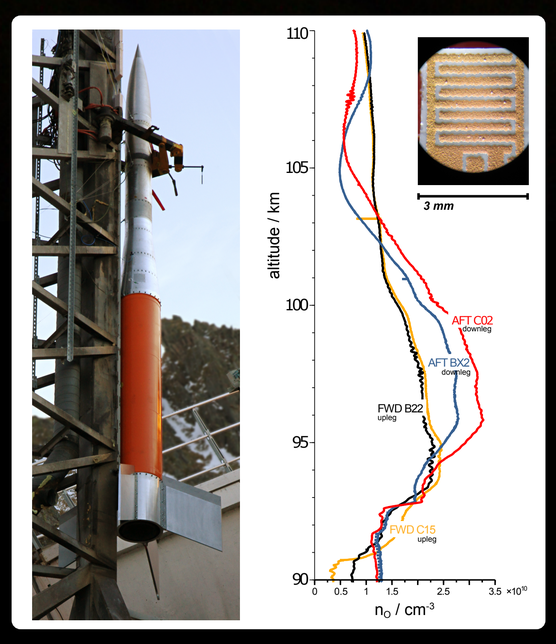

HAYABUSA

Fabry-Perot interferometric measurement of kinetic temperature during re-entry [9].

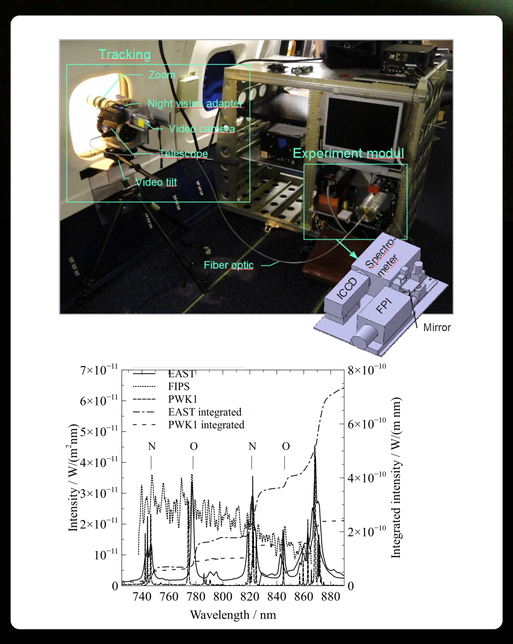

HIFiRE V

Heat flux distribution measurement on a ceramic fin during flight [10].

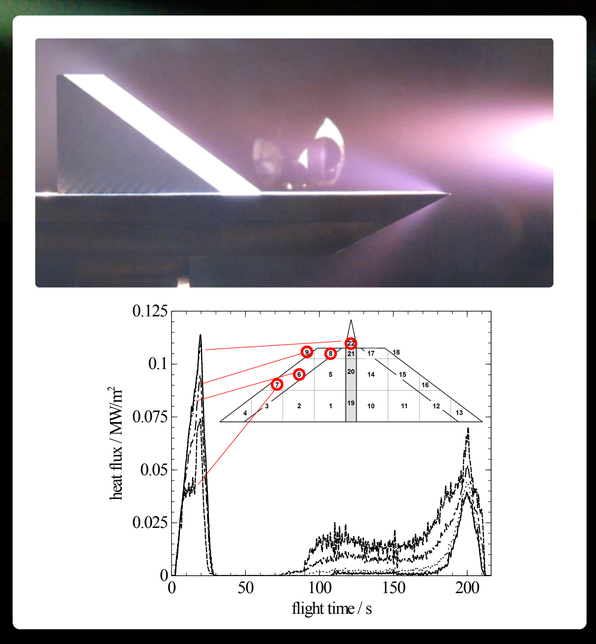

ATV-1

Emission spectroscopy in the UV during airborne observation of the destructive re-entry of ATV-1 [11].

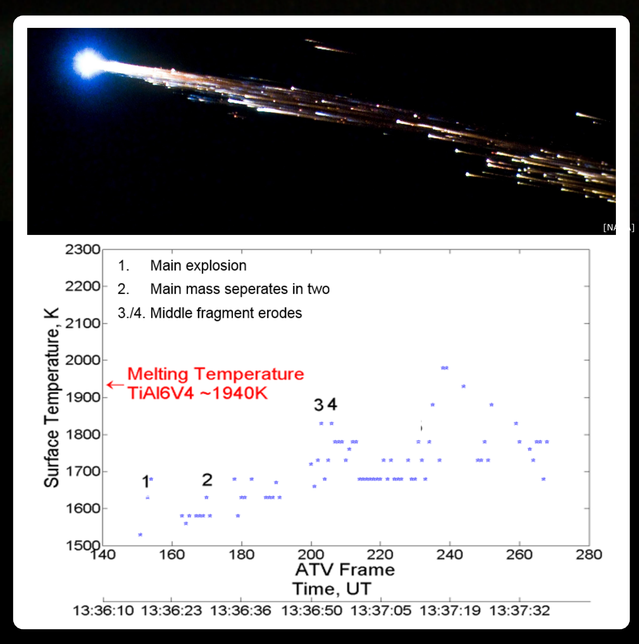

References:

[1] Loehle, S., Staebler, T. Reimer, T., "Photogrammetric Surface Analysis of Ablation Processes in High Enthalpy Air Plasma Flow", AIAA Journal, accepted for publication, 2015
[2] Loehle, S., Fuchs, U., Digel, P., Hermann, T., Battaglia, J.-L., "Analysing Inverse Heat Conduction Problems by the Analysis of the System Impulse Response", Inverse Problems in Science and Engineering, 2014
[3] Loehle, S., Steinbeck, A., Fasoulas, S., "Local Mass-Specific Enthalpy Measurements with a new Mass Injection Probe", AIAA JTHT, in press 2015
[4] Fulge, H., Loehle, S., Fasoulas, S., "Analysis of Wavelength Modulation Spectroscopy for Water Vapour Measurements in Supersonic Combustion", 11th AIAA Thermophysics Conference, Atlanta, 2014.
[5] Marynowski, T., Loehle, S., Fasoulas, S., "Two-Photon Absorption Laser-Induced Fluorescence Investigation of CO_2 Plasmas for Mars Entry", AIAA JTHT, Vol. 28, No. 3, 2014.
[6] Hermann, T., Loehle, S., Zander, F., Fulge, H., and Fasoulas, S., "Characterization of a Re-entry Plasma Wind Tunnel Flow with Vacuum Ultraviolet to Near Infrared Spectroscopy", AIAA JTHT, 2015, submitted.
[7] Zander, F., Marynowski, T., Loehle, S., "High-Speed Imaging of a Steady State CO2 Plasma Flow", AIAA JTHT, 2015, submitted.
[8] Eberhart, M., Loehle, S., Steinbeck, A., Binder, T., and Fasoulas, S., "Measurement of atomic oxygen in the middle atmosphere using solid electrolyte sensors and catalytic probes",Atmos. Meas. Tech. Discuss., Vol. 8, 2015.
[9] Loehle, S., Jenniskens, P., "High-Resolution Spectroscopy of the Hayabusa Reentry Using a Fabry-Perot Interferometer", AIAA JSR, Vol. 51, 2014.
[10] Loehle, S., Boehrk, H., Fuchs, U., Kraetzig, B., Weihs, H., "Three-dimensional Thermal Analysis of the HIFiRE-V Ceramic Fin", 18th AIAA Space Planes and Hypersonic Systems Conference, Tours, 2012
[11] Loehle, S., Wernitz, R., Herdrich, G., Fertig, M., Roeser, H.-P., and Ritter, H., "Airborne Re-entry Observation Experiment SLIT: UV Spectroscopy during Stardust and ATV1 Re-entry", CEAS Space Journal, Vol. 1, 2011.

Acknowledgement: The authors gratefully acknowledge the support of the various efforts through funding by the European Space Agency, the German Research Foundation, and the German Aerospace Center

Contact:
Dr. Stefan Löhle
Institute of Space Systems
Pfaffenwaldring 29
70569 Stuttgart, Germany
e-mail: loehle@irs.uni-stuttgart.de
T: +49 - 711 - 685 - 62387

Cavity–Stabilized Scramjet Analysis Using Reduced Chemical Kinetic Mechanisms

Ramin ROUZBAR, Sinan EYI

Middle East Technical University, 06800, Ankara/TURKEY

Abstract

Air-breathing propulsion is one of the important research fields of the hypersonic flow today. The objective of the present study is to develop a CFD tool to analyze the flow through Scramjets. The configuration considered is a Scramjet with single cavity recessed in the combustion chamber. Cavities are designed to enhance the mixing by means of creating a recirculation region which cause an increase in the residence time and so mixing efficiency. For this CFD tool, Euler equations and finite rate chemistry equations are used. Hydrogen-Air and Ethylene-Air combustion mechanism are considered for Scramjet combustor. For the solution of the coupled Euler and chemical reaction equations Newton-GMRES method is applied. Newton-GMRES is one of the Newton-Krylov solution methods which is a kind of Inexact Newton method.

Introduction

From mid-50's, Scramjets became main area of interest of the air-breathing propulsion systems. Since for hypersonic flow regions decelerating the flow to subsonic speeds causes significant pressure loss and temperature rise ramjets became non-profitable.[1] In Scramjets, air enters the combustion chamber at supersonic speeds and combustion occurs in supersonic flow region. One of the biggest challenges of the scramjet propulsion system is the design of the combustor since the flow must be maintained at supersonic level. Flow compressibility and reduced residence time in the combustor because of the supersonic conditions will cause poor mixing rate of the fuel-air and flame holding will be difficult. In order to overcome the low mixing efficiency cavity is used on the combustion chamber wall. The principle of the use of cavity is that by creating a circulation region in the combustor and so increasing the residence time it improves the mixing efficiency and flame holding.[2] For this study, combustion chamber of the experimental scramjet in research cell 18 at Wright-Patterson Air Force Base is taken as reference. [7]

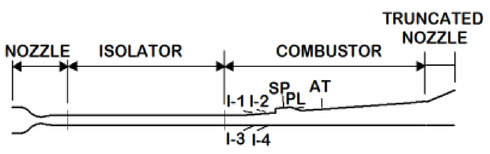

Figure 1. Schematic Scramjet

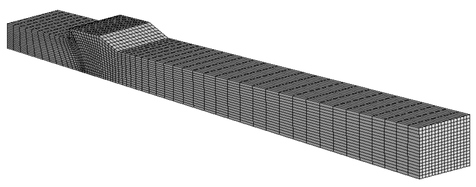

Figure 2. Combustor grid distribution

Methods

To analyze the flow in the combustion chamber, three dimensional coupled equations of Euler and finite rate chemical reactions are used.

$$\frac{\partial \hat{F}(\hat{Q})}{\partial \xi} + \frac{\partial \hat{G}(\hat{Q})}{\partial \eta} + \frac{\partial \hat{H}(\hat{Q})}{\partial \zeta} - \hat{S} = 0$$

$$\hat{Q} = \frac{1}{J}\begin{bmatrix} \rho \\ \rho u \\ \rho v \\ \rho w \\ \rho e_t \\ \rho_1 \\ \vdots \\ \rho_{K-1} \end{bmatrix}, \quad \hat{F} = \frac{1}{J}\begin{bmatrix} \rho U \\ \rho u U + \xi_x p \\ \rho v U + \xi_y p \\ \rho w U + \xi_z p \\ (\rho e_t + p) U \\ \rho_1 U \\ \vdots \\ \rho_{K-1} U \end{bmatrix}, \quad \hat{G} = \frac{1}{J}\begin{bmatrix} \rho V \\ \rho u V + \eta_x p \\ \rho v V + \eta_y p \\ \rho w V + \eta_z p \\ (\rho e_t + p) V \\ \rho_1 V \\ \vdots \\ \rho_{K-1} V \end{bmatrix}, \quad \hat{H} = \frac{1}{J}\begin{bmatrix} \rho W \\ \rho u W + \zeta_x p \\ \rho v W + \zeta_y p \\ \rho w W + \zeta_z p \\ (\rho e_t + p) W \\ \rho_1 W \\ \vdots \\ \rho_{K-1} W \end{bmatrix}, \quad \hat{S} = \frac{1}{J}\begin{bmatrix} 0 \\ 0 \\ 0 \\ 0 \\ 0 \\ \dot{\omega}_1 \\ \vdots \\ \dot{\omega}_{K-1} \end{bmatrix}$$

Spatial discretization of the flux vectors are done using upwind flux vector splitting schemes.

$$\hat{F}_{i\pm1/2,j,k} = \hat{F}^{+}{}_{i\pm1/2,j,k}\left(\hat{Q}^{-}{}_{i\pm1/2,j,k}\right) + \hat{F}^{-}{}_{i\pm1/2,j,k}\left(\hat{Q}^{+}{}_{i\pm1/2,j,k}\right)$$

$$\hat{F}^{\pm} = \pm\frac{1}{J}\,\rho c\,\frac{1}{4}(M \pm 1)^2\left(\tilde{k}_1 + \tilde{k}_2 + \tilde{k}_3\right)\begin{bmatrix} 1 \\ \frac{1}{\gamma}\left(-\tilde{U} \pm 2c\right)\tilde{k}_1 + u \\ \frac{1}{\gamma}\left(-\tilde{U} \pm 2c\right)\tilde{k}_2 + v \\ \frac{1}{\gamma}\left(-\tilde{U} \pm 2c\right)\tilde{k}_3 + w \\ \frac{\tilde{U}}{\gamma+1}\left(-\tilde{U} \pm 2c\right) + \frac{2c}{\gamma^2-1} + \frac{u^2+v^2+w^2}{2} \\ \rho_1/\rho \\ \vdots \\ \rho_{K-1}/\rho \end{bmatrix}$$

The finite rate chemistry model can be expressed as follows for K number of species and I number of the reactions:

$$\sum_{k=1}^{K} \nu'_{k,i}\chi_k \rightleftarrows \sum_{k=1}^{K} \nu''_{k,i}\chi_k \qquad (i = 1,2,..,I)$$

$$k_{fi} = A_i T^{B_i} \exp\left(-E_i/R_u T\right) \qquad k_{bi} = \frac{k_{fi}}{k_{ci}} \qquad k_{ci} = \exp\left(\left(\frac{\Delta S_i}{R} - \frac{\nabla h_i}{RT}\right)\left(\frac{P_{atm}}{RT}\right)^{\sum_{K=1}^{K}\nu_{ki}}\right)$$

$$\dot{\omega}_k = W_k \sum_{i=1}^{I}\left(\nu''_{ki} - \nu'_{ki}\right)\left(k_{fi}\prod_{k=1}^{K}[X_k]^{\nu'_{ki}} - k_{bi}\prod_{k=1}^{K}[X_k]^{\nu''_{ki}}\right)$$

In Newton-GMRES method by using the restriction given in Eq. (25) Newton's methods leads to inexact Newton method.

Table 1. Hydrogen-Air Reaction Rates

Reactions	Forward Reaction		
	A_f	B_f	E_f/R
$H_2 + M \rightleftarrows H + H + M$	2.2×10^{14}	0.0	48300
$O_2 + M \rightleftarrows O + O + M$	9.8×10^{24}	−2.5	59380
$H_2O + M \rightleftarrows OH + H + M$	3.5×10^{15}	0.0	52900
$OH + M \rightleftarrows O + H + M$	8.5×10^{18}	−1.0	50830
$H_2O + O \rightleftarrows OH + OH$	6.8×10^{13}	0.0	9240
$H_2O + H \rightleftarrows OH + H_2$	9.3×10^{13}	0.0	10250
$O_2 + H \rightleftarrows OH + O$	2.2×10^{14}	0.0	8450
$H_2 + O \rightleftarrows OH + OH$	1.8×10^{10}	1.0	4480

Table 2. Ethylene-Air Reaction Rates

Reaction	Forward Reaction		
	A_f	B_f	E_f/R
$C_2H_4 + O_2 \rightleftarrows 2CO + 2H_2$	2.10×10^{14}	0.0	18015.3
$2CO + O_2 \rightleftarrows 2CO_2$	3.48×10^{11}	2.0	10134.9
$2H_2 + O_2 \rightleftarrows 2H_2O$	3.0×10^{20}	−1.0	0.0

In order to solve the coupled Euler equations and finite rate chemistry equations Newton-GMRES is used which is an alternative method with matrix free solution technique. In Newton-GMRES method by using the restriction given, Newton's methods leads to inexact Newton method.

$$\hat{R}(\hat{Q}) = 0 \qquad \left\|\hat{R}(\hat{Q}_k) + \hat{R}'(\hat{Q}_k)\,\Delta\hat{Q}_k\right\| \le \eta_k\left\|\hat{R}(\hat{Q}_k)\right\| \qquad \hat{R}'(\hat{Q}_k)\,\Delta\hat{Q}_k = -\hat{R}(\hat{Q}_k)$$

Results

Liquid Hydrocarbon fuels are more efficient in low hypersonic Mach numbers while Hydrogen is more efficient in high Mach numbers.

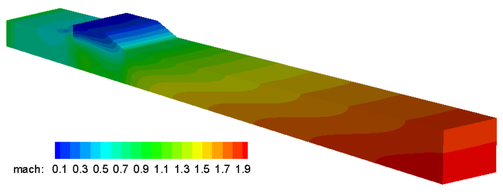

Figure 3. Combustor Mach number variation

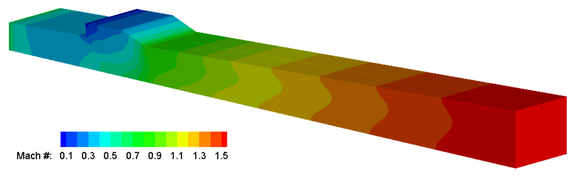

Figure 8. Combustor Mach number variation

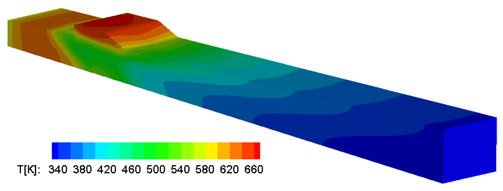

Figure 4. Combustor temperature distribution

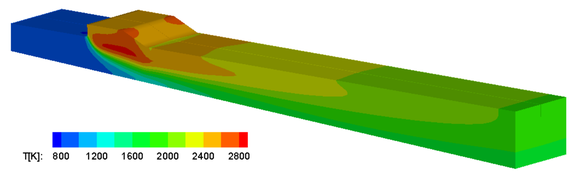

Figure 9. Combustor temperature distribution

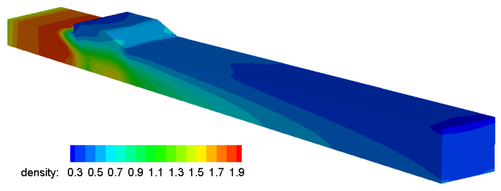

Figure 5. Combustor density distribution

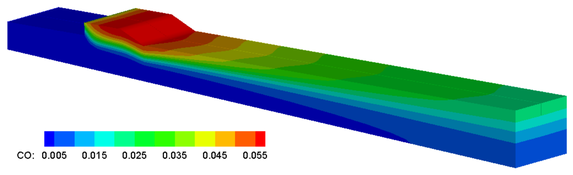

Figure 10. Hydroxide mass fraction

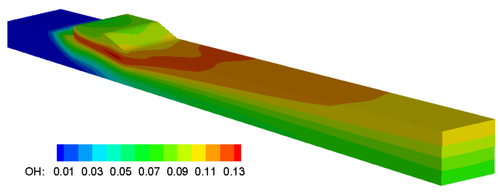

Figure 6. Hydroxide mass fraction

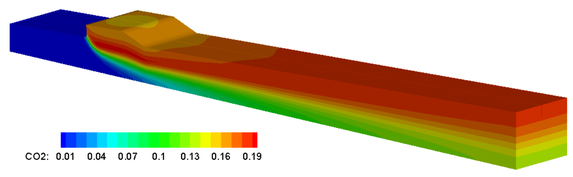

Figure 11. Hydroxide mass fraction

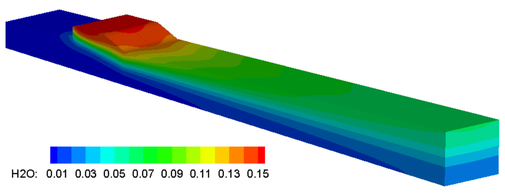

Figure 7. Vapor water mass fraction

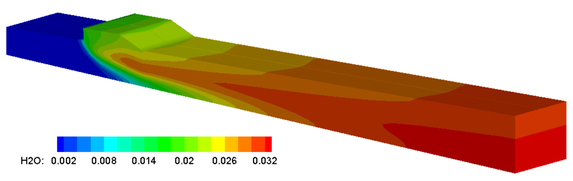

Figure 12. Vapor water mass fraction

Conclusions

Conclusion can be summarized as follows:

- A bow shock has been generated over the fuel injectors where velocity of the main flow decreases and density increased abruptly. Moreover, because of the recirculation region created in the cavity flow slows down further and so Mach number decreases. But, downstream of the cavity, velocity of the flow increased as a consequence of the divergent geometry of the combustion chamber.
- mixing occurs immediately after the injection of the fuel inside the cavity. The combustion process and decreasing flow velocity cause temperature to experience a peak, downstream of the fuel injectors in the cavity region.
- Mass fraction of the products increased after the fuel injection where combustion has occurred which is expected.

Acknowledgement

This research is supported by The Scientific and Technological Research Council of Turkey (TUBITAK).

Bibliography

1. Wang, Z., Wang, H., and Sun, M., "Review of cavity-stabilized combustion for scramjet applications," Proceedings of the Institution of Mechanical Engineers, Part G: Journal of Aerospace Engineering, vol. 228, Feb. 2014, pp. 2718–2735
2. Baurle, R. A., and Eklund, D. R., "Analysis of Dual-Mode Hydrocarbon Scramjet Introduction," vol. 18, 2002.
3. Lin, K., Tam, C., Carter, C., Jackson, K., and Lindsey, M., "Flame Characteristics and Fuel Entrainment Inside a Cavity Flame Holder in a Scramjet Combustor," 2007, pp. 1–19.